ELSEVIER

Chemical Geology 236 (2007) 112–133

CHEMICAL GEOLOGY
INCLUDING
ISOTOPE GEOSCIENCE

www.elsevier.com/locate/chemgeo

Shrimp U–Pb zircon geochronology, geochemistry, and Nd–Sr isotopic study of contrasting granites in the Emeishan large igneous province, SW China

Hong Zhong [a,*], Wei-Guang Zhu [a], Zhu-Yin Chu [b], De-Feng He [a], Xie-Yan Song [a]

[a] *State Key Laboratory of Ore Deposit Geochemistry, Institute of Geochemistry, Chinese Academy of Sciences, 46 Guanshui Road, Guiyang 550002, PR China*

[b] *State Key Laboratory of Lithospheric Evolution, Institute of Geology and Geophysics, Chinese Academy of Sciences, Beijing 100029, PR China*

Received 19 December 2005; received in revised form 29 August 2006; accepted 19 September 2006

Editor: R.L. Rudnick

Abstract

The Cida A-type granitic stock (~4 km^2) and Ailanghe I-type granite batholith (~100 km^2) in the Pan-Xi (Panzhihua-Xichang) area, SW China, are two important examples of granites formed during an episode of magmatism associated with the Permian Emeishan mantle plume activity. This is a classic setting of plume-related, anorogenic magmatism exhibiting the typical association of mantle-derived mafic and alkaline rocks along with silicic units. SHRIMP zircon U–Pb data reveal that the Cida granitic pluton (261±4 Ma) was emplaced shortly before the Ailanghe granites (251±6 Ma). The Cida granitoids display mineralogical and geochemical characteristics of A-type granites including high FeO*/MgO ratios, elevated high-field-strength elements (HFSE) contents and high Ga/Al ratios, which are much higher than those of the Ailanghe granites. All the granitic rocks show significant negative Eu anomalies and demonstrate the characteristic negative anomalies in Ba, Sr, and Ti in the spidergrams. It can be concluded that the Cida granitic rocks are highly fractionated A-type granitoids whereas the Ailanghe granitic rocks belong to highly evolved I-type granites.

The Cida granitoids and enclaves have Nd and Sr isotopic initial ratios ($\varepsilon_{Nd}(t)=-0.25$ to $+1.35$ and $(^{87}Sr/^{86}Sr)_i=0.7023$ to 0.7053) close to those of the associated mafic intrusions and Emeishan basalts, indicating the involvement of a major mantle plume component. The Ailanghe granites exhibit prominent negative Nb and Ta anomalies and weakly positive Pb anomalies in the spidergram and have nonradiogenic $\varepsilon_{Nd}(t)$ ratios (-6.34 to -6.26) and high $(^{87}Sr/^{86}Sr)_i$ values (0.7102 to 0.7111), which indicate a significant contribution from crustal material. These observations combined with geochemical modeling suggest that the Cida A-type granitoids were produced by extensive fractional crystallization from basaltic parental magmas. In contrast, the Ailanghe I-type granites most probably originated by partial melting of the mid-upper crustal, metasedimentary–metavolcanic rocks from the Paleo-Mesoproterozoic Huili group and newly underplated basaltic rocks.

In the present study, it is proposed that petrogenetic distinctions between A-type and I-type granites may not be as clear-cut as previously supposed, and that many compositional and genetically different granites of the A- and I-types can be produced in the plume-related setting. Their ultimate nature depends more importantly on the type and proportion of mantle and crustal material

* Corresponding author. Tel.: +86 851 589 1820; fax: +86 851 589 1664.
E-mail address: zhonghong@vip.gyig.ac.cn (H. Zhong).

doi:10.1016/j.chemgeo.2006.09.004

involved and melting conditions. Significant melt production and possible underplating and/or intrusion into the lower crust, may play an important role in generating the juvenile mafic lower crust (average 20 km) in the central part of the Emeishan mantle plume.

Keywords: Emeishan; SW China; Granite; Petrogenesis; Mantle plume

1. Introduction

The genesis of anorogenic granitoids remains controversial, especially because of the diversity of rocks grouped under that category, commonly termed "A-type" (Eby, 1992). A major characteristic of plume magmatism is the voluminous production of suites of compositionally diverse rocks that are temporally and spatially associated. A-type granitic plutons and felsic volcanics have long been recognized as being associated with continental flood basalt provinces (e.g., Paraná–Etendeka, Siberian and Yemen–Ethiopia igneous provinces; Chazot and Bertrand, 1995; Milner and le Roex, 1996; Peccerillo et al., 2003; Vernikovsky et al., 2003; Frindt et al., 2004), whereas only minor comagmatic I-type granites are reported in the plume-related setting (e.g., Dobretsov and Vernikovsky, 2001). During the upwelling of mantle plumes from the deep mantle, the relative importance of the crust and mantle in the petrogenesis of the small volumes of granitic rocks has been controversial. Considerable debate has also centered on the relative roles of fractional crystallization, assimilation-fractional crystallization (AFC), partial melting and magma mixing in the generation of the felsic magmas.

The Permian Emeishan large igneous province (ELIP), consisting of huge volumes of flood basalts, numerous ultramafic/mafic intrusive rocks, granites, and syenites, is exposed over a large part of SW China from the eastern margin of the Tibetan Plateau to the western margin of the Yangtze block (Fig. 1a). The ELIP has recently been believed to result from the impingement of a mantle plume onto the lithosphere (e.g., Chung and Jahn, 1995; Chung et al., 1998; Xu et al., 2001; Song et al., 2001; He et al., 2003; Xu et al., 2004; Xiao et al., 2004; Fan et al., 2004). A number of studies have focused on the petrogenesis of the Emeishan basalts and the ultramafic/mafic intrusions (Chung and Jahn, 1995; Xu et al., 2001; Song et al., 2001; Zhong et al., 2002, 2003; Xiao et al., 2004; Zhong et al., 2004), whereas the origin and mechanisms of magma emplacement and evolution of the related granites are poorly understood. The Pan-Xi (Panzhihua-Xichang) area in the inner zone of the ELIP (e.g., Xu et al., 2004), is the site of extensive magmatic activity in response to the rising plume head (He et al., 2003). A- and I-types granitoids are correlated in space and time with the ultramafic/mafic layered intrusions and alkalic rocks in the Pan-Xi area, which are all controlled by several regional N–S-trending faults (Fig. 1a; Zhou et al., 1985; Liu et al., 1985). These ultramafic/mafic intrusions have been found to host giant Fe–Ti–V deposits and Cu–Ni–PGE (platinum-group element) sulfide mineralization, including the Panzhihua, Hongge, Baima, Taihe and Xinjie intrusive complexes (Yao et al., 1993; Zhong et al., 2002, 2003, 2004). The different types of granitic rocks in the ELIP constitute a typical example of plume-related granite magmatism because of the large range of compositions produced in the same tectonic and geologic setting and in a very narrow interval of time. Understanding the genesis of these granitoids can contribute toward solving the longstanding controversies about the nature of the A-type granites and evaluate the importance of large mantle upwellings in producing juvenile crust. The possible controlling factors on their compositional diversity also have implications for the broader issue of anorogenic granites in general.

In this paper, we present precise SHRIMP U–Pb zircon ages, geochemical and Nd, and Sr isotope data for the representative Cida A-type and Ailanghe I-type granites in the ELIP (Fig. 1a). The major aims are (1) to elucidate the link between mafic and felsic magmatism in the ELIP; (2) to characterize the chemical and isotopic nature of the mantle responsible for derivation of A- and I-types granites, and (3) to evaluate the role of mantle–lithosphere interaction, and to assess their respective contributions to the construction of crust in the mantle plume-related environment.

2. Geologic setting

The ELIP is located in the western margin of the Yangtze craton, SW China (Fig. 1a). The basement of the Yangtze craton locally comprises the Paleoproterozoic Kangding Complex, composed of granulite–amphibolite facies metamorphic rocks, and the Paleo-Mesoproterozoic Huili Group or its equivalents, the Yanbian or Kunyang Groups, which consists of low-

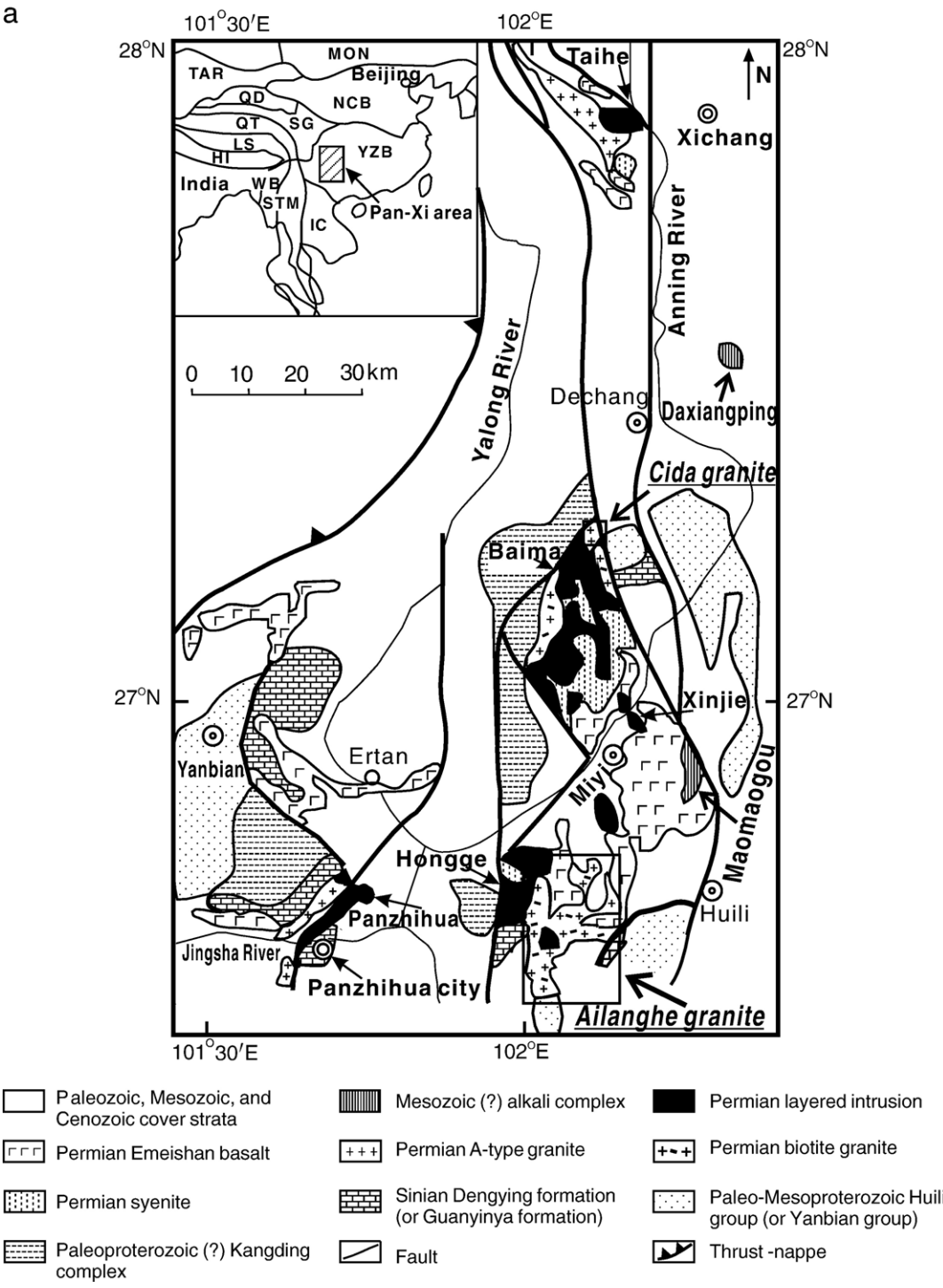

Fig. 1. (a) Geological map of the Pan-Xi area and the distributions of the mafic/ultramafic intrusions, granites, syenites and alkaline complexes (modified after Liu et al., 1985; Cong, 1988). *Insert* illustrates distributions of major terranes in China (modified after Chung and Jahn, 1995), Abbreviations: NCB = North China block; YZB = Yangtze block; SG = Songpan–Ganze accretionary complex; QT = Qiangtang; LS = Lhasa; HI = Himalayan; TAR = Tarim; MON = Mongolia; QD = Qaidam; WB = West Burma; STM = Shan–Thai–Malay; IC = Indochina; (b) Simplified geological map of the Cida granitic intrusion (modified after Zhou et al., 1985); (c) Simlified geological map of the Ailanghe granite batholith (modified after SBGMR, 1991).

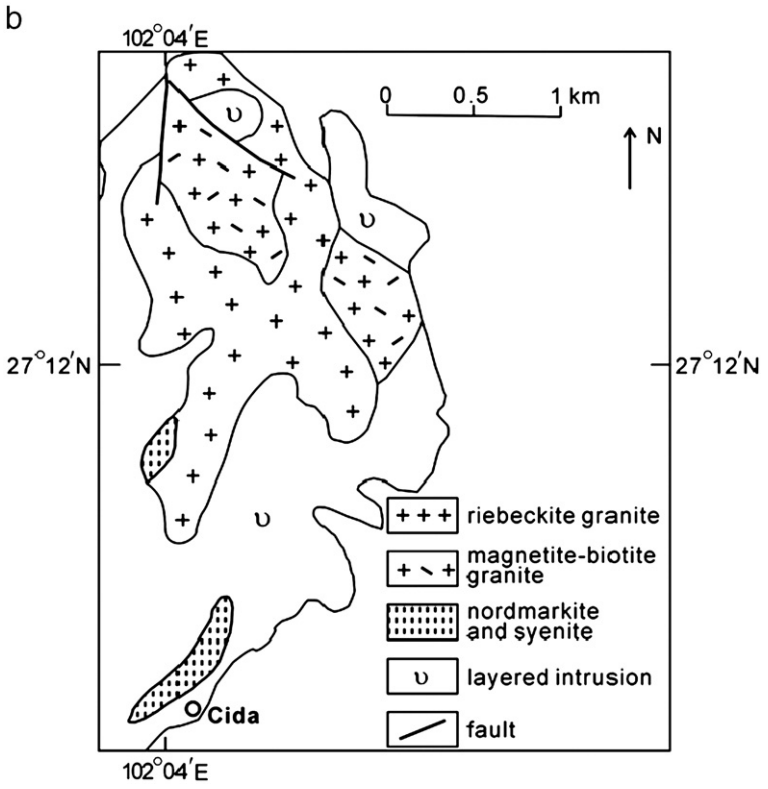

Fig. 1 (*continued*).

grade metasedimentary rocks interbedded with felsic and mafic metavolcanic rocks. The basement is overlain by a thick sequence (>9 km) of Sinian (610–850 Ma) to Permian strata composed of clastic, carbonate, and metavolcanic rocks (SBGMR, 1991). The Emeishan basalts are exposed over a rhombic area of $\sim 2.5 \times 10^5$ km^2. The thickness of the Emeishan volcanic succession varies considerably from over 5000 m in the west to several hundred meters in the east. The whole province consists predominantly of basaltic flows and pyroclastics. Flows and tuffs of trachyte and rhyolite occur in the uppermost sequence of the ELIP (Huang et al., 1986; Chung and Jahn, 1995). The Emeishan basalts unconformably overlie the late Mid-Permian Maokou Formation comprising limestones, and are covered by early Late Permian Longtan Formation or Triassic sedimentary rocks. A mantle plume origin for the ELIP is becoming increasingly accepted by the geologists, as suggested by several recent geological, geochemical and geophysical studies (Chung and Jahn, 1995; Chung et al., 1998; Xu et al., 2001; Song et al., 2001; He et al., 2003; Xu et al., 2004; Xiao et al., 2004).

Generally, the major volume of lava in most LIPs appears to have been erupted over a very short time interval (1–2 Ma), such as in the Siberian, Deccan, and the North Atlantic large igneous provinces (e.g., Courtillot et al., 1986; Kerr, 1994; Renne et al., 1995). Magnetostratigraphic data and field observations suggest that the bulk of the Emeishan volcanic sequence formed within 1–2 Ma (Huang and Opdyke, 1998; Ali et al., 2002). Recent U–Pb SHRIMP and TIMS dating of zircons from several coeval mafic/ultramafic intrusions and a diabasic dike indicate that the ELIP was voluminously erupted at ~260 Ma, consistent with the end-Guadalupian (end Middle Permian) stratigraphic age (Zhou et al., 2002; Guo et al., 2004; Zhong and Zhu, 2006). In contrast, the age of 251–255 Ma for biotite separates from the Panzhihua and Maomaogou syenites (Lo et al., 2002) could correspond to the wanning stage of the ELIP, although ^{40}Ar/^{39}Ar ages for the Emeishan basalts and associated rocks are thought to be problematic possibly due to a monitor standard miscalibration (Ali et al., 2005).

The Pan-Xi area occurs in the inner zone of the ELIP (Xu et al., 2004), which is considered the impact site of the rising plume head (He et al., 2003). The area comprises N–S trending, fault-controlled, massive flood basalts, numerous associated mafic/ultramafic intrusions,

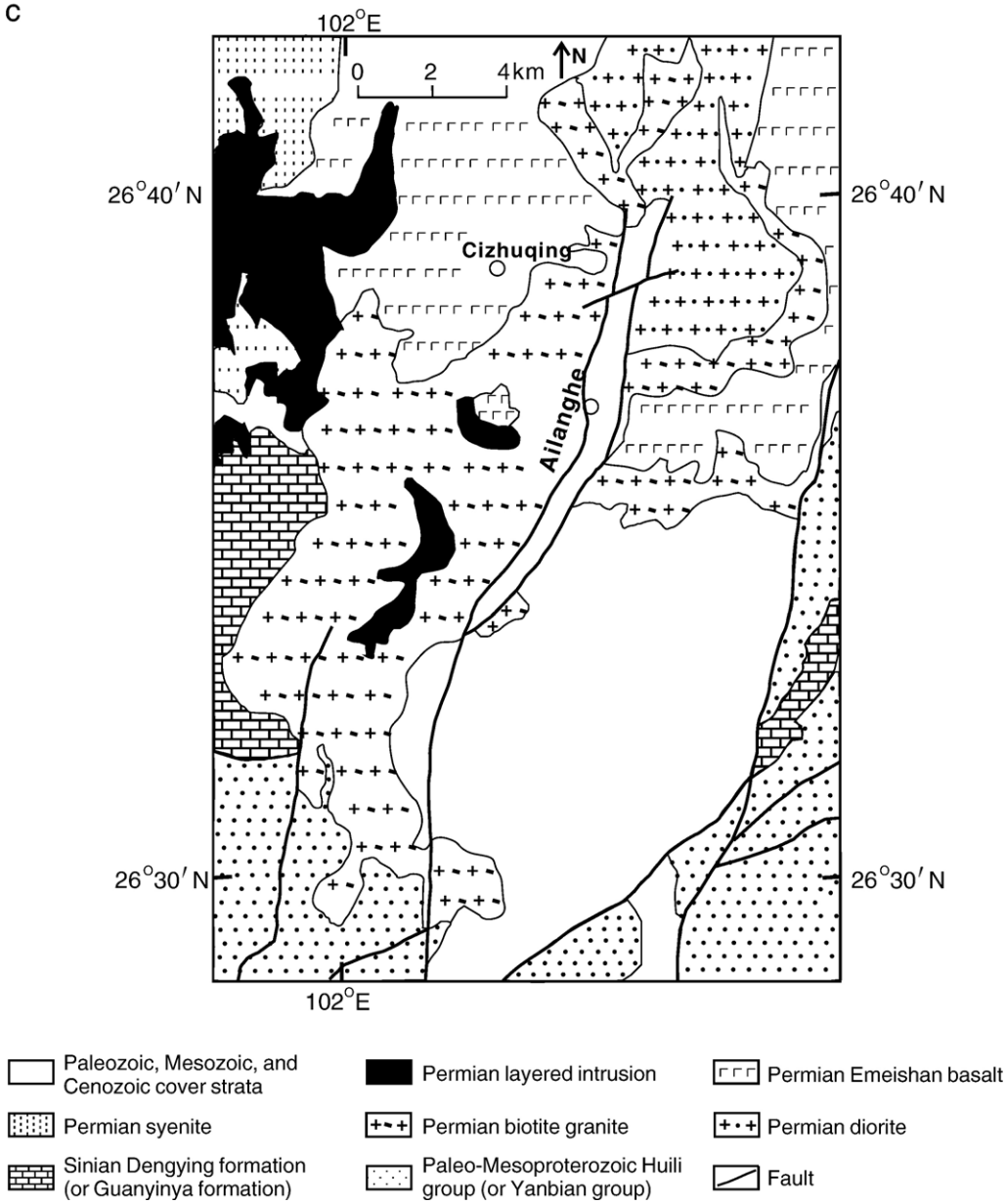

Fig. 1 (*continued*).

and granites and syenites. The mafic/ultramafic intrusions described here are exposed along a 200 km-long belt, having a size ranging from ~1 to 60 km^2 (Fig. 1a). Several large intrusions (~13–60 km^2) host giant V–Ti–magnetite deposits (e.g,, Panzhihua, Hongge, Baima and Taihe) with a total known metal resource of ~5.72×10^9 tonne Fe, >4.66×10^8 tonne Ti, >2.66×10^7 tonne V (Yao et al., 1993) and contain Ni–Cu–PGE sulfide horizons (Zhong et al., 2002, 2003, 2004). Many small intrusions contain Ni–Cu–PGE sulfide deposits (e.g., Yangliuping, Limahe and Jinbaoshan) (Song et al., 2003; Tao et al., 2002).

The Emeishan plume-related granites, including the Taihe (~50 km^2), Panzhihua (~20 km^2), and Cida (~4 km^2) stocks, and the Ailanghe batholith (~100 km^2) (Zhou et al., 1985; Zhang et al., 1988) (Fig. 1a), are all associated with the relatively large mafic/ultramafic layered intrusions hosting giant Fe–Ti–V deposits (Fig. 1a). Several alkaline ring complexes spatially and temporally related to the ELIP also occur

in the Pan-Xi area, namely, the Daxiangping (~6 km^2; Fig. 1a), Liushaxiang (~4.2 km^2), Maomaogou (~32 km^2; Fig. 1a), and Jijie (~0.32 km^2) complexes from the north to the south. Zhou et al. (1985) suggested that the granites and syenites in the Pan-Xi area represent the very final stage of the Emeishan plume activity. Most of the A-type granite and syenite bodies of diverse composition in the area intruded the Emeishan basalts and mafic/ultramafic intrusions. The stocks comprise predominantly riebeckite granite, aegirine granite, and nordmarkite, whereas the batholith mainly consists of biotite K-feldspar granite. The different characteristics may correspond to various petrogenetic processes, as will be shown below.

3. Petrography

This study is focused on the Cida A-type and Ailanghe I-type granitoid bodies, which are typical in mode of occurrence, composition, and size. The Cida granitoid stock is about 3.1 km long and 1.4 km wide (Zhou et al., 1985) and is genetically related to the Baima mafic/ultramafic intrusion (~50 km^2) hosting giant V–Ti magnetite deposits. These granitoids were emplaced in the northeastern part of the Baima mafic intrusion (Fig. 1b). The Cida granitic intrusion comprises dominant riebeckite granite, subordinate magnetite–biotite granite, and less abundant nordmarkite and horblende syenite only occurring at the margins. These rocks have medium, graphic and porphyritic textures. The principal mineralogy consists of perthite, quartz, riebeckite and biotite. Nordmarkite, as compared with syenite, is richer in quartz (5–7%) and mafic mineral (riebeckite; 3–5%). The main rock-forming mineral is also a mesoperthitic alkali feldspar. Overgrowths of riebeckite on the salite and amphibole grains suggest their crystallization at the magmatic stage. The common accessories include fergusonite, zircon, sphene, allanite, thorite, orvillite, cyrtolite. Abundant gabbroic and dioritic enclaves, and mafic dikes occur near the margins

Table 1
SHRIMP zircon U–Pb isotopic analyses of the Cida and Ailanghe granites

Spot	$^{206}Pb_c$	U	Th	Th/U	$^{206}Pb^*$	$^{207}Pb^*/^{206}Pb^*$	±%	$^{207}Pb^*/^{235}U$	±%	$^{206}Pb^*/^{238}U$	±%	$^{206}Pb^*/^{238}U$
	[%]	[ppm]	[ppm]		[ppm]							[age, Ma]
CD0401												
1.1	0.40	270	114	0.44	9.90	0.0540	4.0	0.317	5.2	0.0426	3.2	268.8±8.5
2.1	0.19	1480	1444	1.01	53.7	0.0502	1.9	0.292	3.7	0.0422	3.2	266.2±8.2
3.1	0.10	1413	1338	0.98	49.8	0.0521	1.0	0.295	3.3	0.0410	3.2	259.1±8.0
4.1	0.09	2021	2292	1.17	71.3	0.0515	1.0	0.291	3.3	0.0410	3.2	259.1±8.0
5.1	0.06	771	556	0.74	27.5	0.0527	1.4	0.302	3.5	0.0415	3.2	262.4±8.2
6.1	0.55	578	414	0.74	20.1	0.0477	3.6	0.265	4.8	0.0403	3.2	254.7±8.0
7.1	0.15	1010	890	0.91	36.4	0.0507	1.4	0.293	3.5	0.0419	3.2	264.7±8.2
8.1	0.14	853	665	0.81	29.6	0.0512	1.8	0.285	3.7	0.0404	3.2	255.4±8.0
9.1	0.10	2441	3381	1.43	84.7	0.0517	1.0	0.287	3.5	0.0403	3.3	254.9±8.3
10.1	0.11	946	722	0.79	33.9	0.0525	3.0	0.301	4.4	0.0416	3.2	262.7±8.2
11.1	0.07	2180	3080	1.46	84.2	0.0515	0.9	0.319	6.8	0.0449	6.8	283±19
12.1	0.17	1106	692	0.65	39.8	0.0506	1.3	0.292	3.6	0.0418	3.3	264.2±8.5
13.1	0.07	1488	1258	0.87	52.6	0.0502	2.1	0.285	3.8	0.0412	3.2	260.0±8.0
14.1	0.19	789	563	0.74	27.9	0.0518	1.7	0.294	3.6	0.0411	3.2	259.8±8.1
15.1	0.03	1733	2112	1.26	69.4	0.0514	0.9	0.330	4.6	0.0466	4.6	294±13
ALH0401												
1.1	0.15	1128	600	0.55	38.0	0.0517	1.1	0.279	3.4	0.0392	3.2	247.7±7.7
2.1	0.09	711	472	0.69	23.6	0.0517	1.6	0.276	3.6	0.0387	3.2	244.6±7.7
3.1	0.02	2607	909	0.36	88.9	0.0501	1.8	0.274	3.7	0.0397	3.2	251.0±7.9
4.1	0.11	1631	458	0.29	58.8	0.0528	1.1	0.305	3.3	0.0419	3.2	264.9±8.2
5.1	0.05	1659	852	0.53	59.9	0.0500	2.8	0.290	4.2	0.0420	3.2	265.5±8.2
6.1	0.18	1484	842	0.59	51.2	0.0516	1.2	0.285	3.4	0.0400	3.2	253.1±7.8
7.1	0.03	1390	748	0.56	48.4	0.0518	1.1	0.290	3.3	0.0405	3.2	256.1±7.9
8.1	0.23	829	467	0.58	26.9	0.0516	2.6	0.268	4.1	0.0377	3.2	238.3±7.4
9.1	0.13	638	419	0.68	21.4	0.0536	1.6	0.288	3.6	0.0390	3.2	246.5±7.7
10.1	0.32	1018	528	0.54	33.8	0.0505	2.3	0.268	3.9	0.0385	3.2	243.5±7.6
11.1	0.18	606	393	0.67	21.0	0.0517	1.8	0.287	3.7	0.0403	3.2	255.0±8.0

(1) Errors are 1σ; Pb_C and Pb* indicate the common and radiogenic portions, respectively; (2) Error in Standard calibration was 1.29% (not included in above errors but required when comparing data from different mounts); (3) Common Pb corrected using measured ^{204}Pb.

of the Cida granite, which are fine-grained to slightly porphyric rocks.

The Ailanghe granite batholith crops out over an area of 100 km^2 and intruded the giant Fe–Ti–V deposit-bearing Hongge mafic/ultramafic intrusion (~60 km^2) and the adjacent Emeishan basalts (Fig. 1c). The batholith is composed of coarse- to medium-grained biotite K-feldspar granite and medium- to fine-grained monzonitic granite, of which the former are dominant. The batholith was considered to be I-type granitic intrusion on the basis of major element characteristics (Cong, 1988). The Ailanghe granites also intruded the Sinian (610–850 Ma) limestones and the upper part of the Paleo-Mesoproterozoic Huili Group consisting of metasedimentary rocks with interbedded metavolcanic rocks (Fig. 1a). The granites cut the mafic/ultramafic intrusion and thus caused hornfels contact metamorphism and formed a fine-grained marginal zone (SBGMR, 1991). The granitic dikes also intruded the Emeishan basalts. The rocks are characterized by equigranular and coarse- to fine-grained textures. The Ailanghe granite consists predominantly of K-feldspar barbierite (30–60%), quartz (25–40%), plagioclase (10–20%; An=5–21; Cong, 1988), minor microcline (<5%) and biotite (1–3%), and accessory minerals including magnetite, zircon and apatite.

4. Analytical methods

Zircon grains from samples CD0401 and ALH0401 were separated using conventional heavy liquid and magnetic techniques. Representative zircon grains were handpicked under binocular microscope and mounted in an epoxy resin disc, and then polished and coated with gold film. Zircons were documented with transmitted and reflected light micrographs as well as cathodoluminescence (CL) images to reveal their external and internal structures. The U–Pb isotopic analyses were performed using the Sensitive High-Resolution Ion Microprobe (SHRIMP-II) at the Chinese Academy of Geological Sciences (Beijing). Details of the analytical procedures of zircons using SHRIMP were described by Compston et al. (1992) and Song et al. (2002). Inter-element fractionation ion emission of zircon was corrected relative to the RSES reference TEMORA 1 (417 Ma; Black et al., 2003). The uncertainties in ages are cited as 1σ, and the weighted mean ages are quoted at the 95% confidence level (2σ).

Major elements were determined by PANalytical Axios-advance X-ray fluorescence spectrometer (XRF) at the State Key Laboratory of Ore Deposit Geochemistry, Institute of Geochemistry, Chinese Academy of Sciences, using fused lithum-tetraborate glass pellets. Analytical precision as determined on the Chinese National standard GSR-1 was generally around 1–5% (Table 2). Trace elements were analyzed using a Perkin-Elmer Sciex ELAN 6000 ICP-MS at the Guangzhou Institute of Geochemistry, Chinese Academy of Sciences. The powdered samples (50 mg) were dissolved in high-pressure Teflon bombs using HF+HNO_3 mixture for 48 h at ~190 °C (Qi et al., 2000). Rh was used as an internal standard to monitor signal drift during counting. The international standards GBPG-1, OU-6, and the Chinese National standard GSR-1 were used for analytical quality control (Table 2). The analytical precision is generally better than 5% for trace elements. Samples for Sr and Nd isotopic analysis were dissolved in Teflon bombs with HF+HNO_3 acid, and separated by conventional cation-exchange techniques. The isotopic measurements were performed on a Finnigan MAT 262 multi-collector mass spectrometer at the Laboratory for Radiogenic Isotope Geochemistry, Institute of Geology and Geophysics (Beijing), Chinese Academy of Sciences. The measured $^{87}Sr/^{86}Sr$ and $^{143}Nd/^{144}Nd$ ratios are normalized to $^{86}Sr/^{88}Sr=0.1194$ and $^{146}Nd/^{144}Nd=0.7219$, respectively. The $^{87}Sr/^{86}Sr$ ratios of the NBS987 and NBS607 Sr standards and

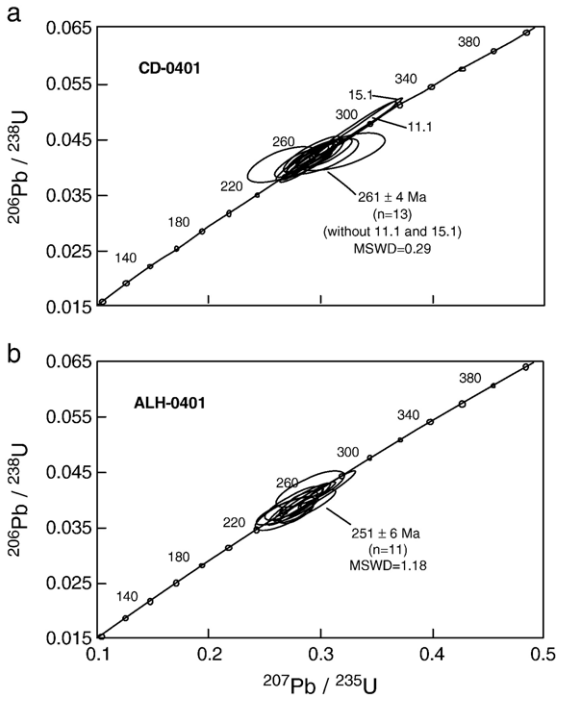

Fig. 2. SHRIMP zircon U–Pb concordia diagram for the granitic rocks (a) Cida granitic pluton; (b) Ailanghe granitic pluton.

Table 2
Major (in wt.%) and trace element (in ppm) data for the Cida and Ailanghe granitic rocks

Sample no.	CD-0401	CD-0402	CD-0403	CD-0404	BM-0405	BM-0406	ALH-0501	ALH-0502	ALH-0503	ALH-0504
Rock type	Granite	Granite	Granite	Nordmarkite	Nordmarkite	Nordmarkite	Granite	Nordmarkite	Granite	Granite
SiO_2	71.76	72.01	72.20	63.38	62.24	61.97	75.82	63.28	72.58	75.56
TiO_2	0.42	0.44	0.45	0.77	0.84	1.06	0.15	0.71	0.29	0.16
Al_2O_3	12.58	12.65	12.57	15.13	14.79	13.86	11.62	14.34	12.55	11.95
Fe_2O_3	3.82	4.18	3.95	7.35	6.69	7.30	2.36	7.55	3.02	2.30
MnO	0.05	0.07	0.06	0.17	0.16	0.13	0.03	0.29	0.07	0.06
CaO	0.79	0.70	0.41	2.16	2.63	3.19	0.19	1.56	0.51	0.31
MgO	0.27	0.25	0.14	0.84	1.17	1.88	0.09	0.26	0.16	0.09
K_2O	5.18	5.64	5.53	5.56	4.91	3.72	4.69	5.44	5.28	4.97
Na_2O	3.76	3.52	3.40	4.19	4.27	4.27	3.72	5.41	3.90	3.63
P_2O_5	0.06	0.06	0.04	0.17	0.20	0.26	0.02	0.13	0.03	0.02
LOI	0.55	0.57	0.85	0.54	0.65	0.97	0.71	0.72	0.91	0.52
Total	99.24	100.09	99.59	100.26	98.56	98.62	99.40	99.68	99.29	99.56
V	16.0	20.6	22.5	32.7	44.9	128	3.44	–	4.89	2.13
Cr	6.23	–	6.92	5.80	4.98	2.95	–	12.3	3.52	–
Co	2.21	2.32	2.46	5.92	7.84	15.6	0.72	1.15	1.09	0.64
Ni	1.01	1.23	5.34	2.93	3.81	7.26	–	7.06	2.67	–
Ga	22.8	24.5	23.9	27.9	26.3	26.0	24.7	28.0	25.8	25.8
Rb	94.2	108	89.1	89.9	79.6	102	191	96.5	177	169
Sr	56.9	52.6	34.6	92.0	108	162	15.0	8.5	17.7	12.6
Zr	1326	1650	1484	477	337	201	751	280	923	701
Nb	48.0	53.5	46.3	78.3	65.9	65.3	116	56.8	84.4	76.0
Cs	0.75	0.72	0.87	0.60	0.92	0.88	0.82	1.18	1.30	1.11
Ba	207	214	196	255	343	535	45.5	78.8	105	64.8
Hf	23.7	30.3	26.7	12.4	9.25	6.77	20.7	8.03	19.6	16.9
Ta	1.87	2.00	1.82	3.14	3.00	4.69	7.93	3.02	5.07	5.29
Pb	8.48	9.03	8.59	12.8	10.3	10.9	16.8	5.77	11.0	10.2
Th	33.3	38.9	30.2	25.9	16.2	15.4	51.3	11.8	38.4	35.4
U	2.33	2.80	2.46	1.22	1.29	2.69	10.26	2.05	5.02	6.10
La	191	233	102	183	102	73.8	67.5	90.1	137	65.2
Ce	398	475	225	363	186	133	143	152	311	144
Pr	37.7	45.7	21.0	35.8	26.2	17.0	14.6	19.4	28.6	15.1
Nd	128	152	71.6	129	103	62.9	51.0	73.9	97.6	54.2
Sm	19.7	23.6	11.6	20.0	18.6	11.4	11.3	12.9	16.6	11.6
Eu	0.80	0.86	0.69	1.58	1.70	1.64	0.23	1.79	0.56	0.32
Gd	17.9	21.4	10.4	19.2	17.3	10.5	11.7	12.6	15.1	11.6
Tb	2.29	2.71	1.41	2.79	2.80	1.76	2.23	2.01	2.21	2.15
Dy	12.4	15.0	8.05	16.4	16.6	10.8	14.5	12.2	13.3	14.2
Ho	2.38	2.87	1.61	3.23	3.19	2.11	2.77	2.27	2.40	2.70
Er	6.77	8.45	4.95	9.62	9.28	7.16	8.89	7.31	7.75	8.90
Tm	0.91	1.16	0.74	1.32	1.31	1.06	1.28	1.05	1.09	1.31
Yb	6.69	8.11	5.51	8.83	8.81	7.74	8.47	7.83	8.04	9.30
Lu	1.03	1.26	0.90	1.31	1.35	1.15	1.16	1.24	1.23	1.36
Y	55.7	64.1	37.3	79.0	77.8	57.4	74.7	58.0	56.3	66.8
δEu	0.13	0.12	0.19	0.25	0.29	0.46	0.06	0.43	0.11	0.08
T_{Zr} (°C)	1067	1100	1091	–	–	–	1002	–	1020	993

Sample no.	CDG-0505	CDG-0506	CDG-0507	CDG-0508	BMG-0501	BMG-0502	ALH-0401	ALH-0402	ALH-0403	ALH-0501
Rock type	Granite	Granite	Granite	Nordmarkite	Enclave	Enclave	Granite	Granite	Granite	Granite
SiO_2	75.07	74.34	74.62	65.44	50.30	59.40	75.35	72.60	72.64	74.79
TiO_2	0.23	0.22	0.22	0.69	1.55	1.07	0.19	0.23	0.22	0.23
Al_2O_3	12.16	11.67	11.87	13.42	15.11	13.96	13.28	13.74	13.56	12.90
Fe_2O_3	2.91	2.91	2.77	7.67	11.52	8.01	1.22	1.80	1.60	1.91
MnO	0.06	0.06	0.05	0.28	0.17	0.13	0.02	0.02	0.02	0.03
CaO	0.40	0.45	0.36	1.48	10.07	6.74	0.44	0.59	0.88	1.12

(continued on next page)

Table 2 (*continued*)

Sample no.	CDG-0505	CDG-0506	CDG-0507	CDG-0508	BMG-0501	BMG-0502	ALH-0401	ALH-0402	ALH-0403	ALH-0501
Rock type	Granite	Granite	Granite	Nordmarkite	Enclave	Enclave	Granite	Granite	Granite	Granite
MgO	0.14	0.14	0.11	0.17	6.78	4.36	0.26	0.37	0.32	0.31
K_2O	4.67	4.71	4.82	5.11	1.11	1.84	5.65	5.48	5.72	4.87
Na_2O	4.13	3.84	3.91	5.35	2.80	4.12	3.60	3.66	3.50	3.19
P_2O_5	0.03	0.03	0.03	0.09	0.32	0.22	0.06	0.07	0.07	0.07
LOI	0.43	0.59	0.51	0.58	1.57	1.08	0.76	1.02	1.07	0.92
Total	100.22	98.96	99.27	100.29	101.31	100.93	100.82	99.58	99.60	100.27
V	5.12	3.66	4.07	–	251	162	5.23	9.63	7.57	11.9
Cr	–	3.44	–	–	104	166	5.12	8.27	6.19	9.56
Co	0.80	1.11	0.80	0.87	42.8	28.0	1.30	2.03	1.63	2.27
Ni	–	0.80	–	–	74.9	55.8	4.24	5.94	3.51	4.09
Ga	26.4	26.5	23.0	29.7	18.1	20.0	13.6	17.2	15.9	15.6
Rb	168	169	172	113	42.8	86.5	190	198	196	190
Sr	14.9	15.8	13.7	6.7	340	168	110	112	184	106
Zr	1034	973	951	308	145	205	128	158	161	175
Nb	78.4	88.5	76.0	77.7	18.6	38.4	20.7	23.6	24.5	25.7
Cs	0.93	1.30	0.93	1.06	0.93	0.92	1.58	2.35	1.63	4.63
Ba	60.2	65.4	60.9	38.3	349	228	403	396	425	316
Hf	21.7	21.0	20.3	9.14	4.01	6.64	5.06	6.01	6.26	5.04
Ta	5.64	5.63	5.10	4.03	1.16	2.86	2.66	3.04	2.82	2.36
Pb	6.79	7.48	7.93	6.72	4.00	9.10	16.9	21.1	20.0	27.2
Th	38.5	38.8	34.5	14.5	5.31	24.3	50.7	45.0	47.9	43.1
U	5.55	6.21	5.48	2.51	1.01	4.07	6.56	7.63	8.40	9.92
La	102	116	103	111	24.1	43.1	106	74.4	93.7	57.0
Ce	197	208	193	186	47.0	77.1	186	131	163	101
Pr	22.6	24.7	21.9	25.6	5.96	9.20	20.4	14.4	18.3	10.9
Nd	77.3	89.4	77.8	95.1	24.2	34.7	64.5	46.1	58.3	38.7
Sm	15.2	17.4	15.0	16.7	5.32	7.03	9.29	7.45	9.37	6.83
Eu	0.33	0.39	0.33	1.39	1.58	1.17	0.52	0.68	0.63	0.50
Gd	14.5	16.1	14.3	14.8	5.53	7.41	7.80	6.43	7.91	5.32
Tb	2.39	2.77	2.32	2.37	0.98	1.37	0.93	0.85	1.07	0.75
Dy	15.0	17.2	14.5	14.3	6.18	8.88	4.95	4.60	5.69	4.47
Ho	2.83	3.29	2.70	2.64	1.18	1.77	0.86	0.85	1.05	0.89
Er	9.16	10.6	8.68	8.67	3.70	5.66	2.50	2.58	2.95	2.73
Tm	1.35	1.56	1.22	1.28	0.51	0.82	0.32	0.37	0.40	0.41
Yb	9.82	11.6	8.79	9.88	3.58	5.83	2.23	2.61	2.66	2.91
Lu	1.47	1.75	1.28	1.62	0.52	0.84	0.31	0.37	0.38	0.45
Y	75.7	84.4	66.1	64.9	30.2	45.3	20.3	21.6	24.5	25.2
δEu	0.07	0.07	0.07	0.27	0.89	0.50	0.19	0.30	0.22	0.25
T_{Zr} (°C)	1034	1039	1029	–	–	–	813	832	830	842

Sample no.	ALH-0502	ALH-0503	ALH-0504	ALH-0505	ALH-0506	GSR-1	RV*	GBPG-1	RV*	OU-6	RV*
Rock type	Granite	Granite	Granite	Granite	Granite	This study		This study		This study	
SiO_2	74.07	74.22	73.84	74.01	73.91	72.51	72.83				
TiO_2	0.23	0.16	0.19	0.24	0.20	0.28	0.29				
Al_2O_3	12.88	12.88	13.07	13.11	13.22	13.52	13.40				
Fe_2O_3	1.54	1.25	1.42	2.67	1.65	2.15	2.14				
MnO	0.02	0.02	0.02	0.05	0.02	0.06	0.06				
CaO	0.61	0.84	0.76	0.85	0.59	1.49	1.55				
MgO	0.25	0.18	0.21	0.30	0.30	0.41	0.42				
K_2O	5.49	5.65	5.44	5.04	5.09	5.01	5.01				
Na_2O	3.47	3.06	3.58	3.63	3.57	3.30	3.13				
P_2O_5	0.07	0.04	0.05	0.07	0.06	0.10	0.09				
LOI	0.78	1.15	1.07	0.77	1.18	0.78	0.76				
Total	99.34	99.42	99.59	100.66	99.74	99.61	99.68				

Table 2
Major (in wt.%) and trace element (in ppm) data for the Cida and Ailanghe granitic rocks

Sample no.	ALH-0502	ALH-0503	ALH-0504	ALH-0505	ALH-0506	GSR-1	RV*	GBPG-1	RV*	OU-6	RV*
Rock type	Granite	Granite	Granite	Granite	Granite	This study		This study		This study	
V	8.26	8.52	10.2	11.7	9.77	22.2	24	96.5	97	132	130
Cr	132	12.3	12.3	15.5	13.4	3.91	5	181	179	71.4	70.7
Co	2.57	1.41	1.63	2.17	2.54	2.77	3.4	19.5	20.1	30.6	29.2
Ni	49.6	3.21	1.80	3.49	3.15	2.24	2.3	58.5	61	37.6	40.2
Ga	12.1	13.7	13.2	15.3	15.3	18.4	19	18.6	18.7	26.7	24.2
Rb	203	217	211	202	197	487	466	56.2	54.7	124	121
Sr	104	93.0	122	144	115	99.2	106	363	364	128	132
Zr	188	80.9	144	169	153	162	167	232	232	165	174
Nb	26.9	20.0	23.5	31.2	27.0	40.0	40	9.9	9.7	13.9	14.5
Cs	2.87	5.62	3.31	2.78	3.62	36.6	38.4	0.32	0.32	7.92	8.10
Ba	366	256	268	366	302	324	313	882	910	462	480
Hf	5.49	2.35	4.22	4.85	4.64	6.48	6.3	6.3	5.9	4.70	4.70
Ta	2.25	1.93	2.43	3.02	2.75	6.96	7.2	0.39	0.41	1.01	1.02
Pb	19.3	32.4	21.2	20.5	26.1	31.4	31	15.6	14.6	27.6	28.8
Th	48.4	99.6	76.4	45.8	36.0	53.3	54	11.8	11.2	11.4	11.3
U	7.77	17.9	16.6	11.9	7.68	18.2	18.8	0.96	0.81	1.91	1.92
La	66.9	44.6	50.2	74.1	51.8	52.1	54	51.1	53	32.5	33.2
Ce	114	81.7	89.4	134	94.6	107	108	103	100	77.9	77.1
Pr	11.9	8.61	9.44	13.3	10.0	13.2	12.7	11.1	11.5	7.64	7.91
Nd	43.0	31.0	34.8	49.6	35.2	48	47	44.5	42	30.5	30.2
Sm	6.85	5.22	6.12	8.13	6.48	10.1	9.7	6.6	6.8	5.99	6.01
Eu	0.47	0.47	0.52	0.57	0.46	0.83	0.85	1.79	1.78	1.39	1.36
Gd	4.92	3.89	4.88	6.52	4.86	9.3	9.3	4.78	4.6	5.37	5.30
Tb	0.67	0.50	0.69	0.95	0.71	1.67	1.65	0.58	0.59	0.89	0.86
Dy	3.96	2.98	4.48	5.92	4.33	10.9	10.2	3.25	3.3	5.02	5.06
Ho	0.74	0.58	0.87	1.16	0.91	2.07	2.05	0.67	0.69	1.04	1.04
Er	2.33	1.66	2.69	3.67	2.67	6.48	6.5	1.93	2.04	2.95	2.93
Tm	0.35	0.25	0.44	0.60	0.41	1.04	1.06	0.30	0.33	0.46	0.45
Yb	2.42	1.69	3.12	4.03	3.01	7.53	7.4	2.04	2.02	2.94	2.98
Lu	0.36	0.24	0.46	0.62	0.45	1.12	1.15	0.31	0.3	0.47	0.45
Y	20.6	15.6	24.6	33.9	24.3	60.6	62	17.0	17.3	25.1	27.8
δEu	0.25	0.32	0.29	0.24	0.25						
T_{Zr} (°C)	847	771	821	837	830						

"–": not determined. Note that T_{Zr} is calculated from zircon saturation thermometry (Watson and Harrison, 1983). RV*: recommended values; The values for GSR-1 from Govindaraju (1994), GBPG-1 from GeoREM (Jochum et al., 2005), and OU-6 from Potts and Kane (2005).

$^{143}Nd/^{144}Nd$ ratios of the BCR-1 and La Jolla Nd standards determined during this study were 0.710265±10 (2σ), 1.200468±17 (2σ), 0.512624±11 (2σ), and 0.511852±6 (2σ), respectively.

5. Results

5.1. U–Pb zircon age

Riebeckite granite sample CD0401 and biotite K-feldspar granite sample ALH0401 were collected from the Cida A-type granitoids and Ailanghe I-type granites in the Pan-Xi area, and the results of SHRIMP zircon U–Pb analyses are listed in Table 1. Zircon grains in CD0401 are clear, euhedral prismatic grains with simple internal growth zonation. Apart from two analyses of slightly older grains (11.1 and 15.1) due to large analytical uncertainties, the remainder 13 SHRIMP analyses for this sample give to a mean $^{206}Pb/^{238}U$ age of 261±4 Ma (2σ; Table 1 and Fig. 2a). Zircon grains in ALH0401 have simple prismatic igneous shapes and magmatic oscillatory zonings. Eleven analyses of zircons from sample ALH0401 yield $^{206}Pb/^{238}U$ single age population of 238 to 266 Ma, with a weighted mean age of 251±6 Ma (2σ; Table 1 and Fig. 2b).

5.2. Major and trace elements

Major and trace element data for the Cida granites, nordmarkites, gabbroic and dioritic enclaves, and Ailanghe granites are given in Table 2, and major oxide contents are illustrated in Figs. 3 and 4. In the present study, the Cida granitoid stock covers a range in SiO_2 from 62.2 to 75.8 wt.% and the Ailanghe granites

have SiO_2 contents ranging from 72.6 to 75.4 wt.%. Chemical analyses show that these rocks have high K_2O (3.7–5.7%), moderate to high Na_2O (3.1–5.4%) and Al_2O_3 (11.6–15.1%). The gabbroic and dioritic enclaves have high FeO* (8.0–11.5%), MgO (4.4–6.8%), CaO (6.7–10.1%), V (162–251 ppm), and Cr (104–166 ppm). Most granitic samples are plotted in the alkaline field on the total alkali–silica (TAS) diagram (Fig. 3a). In a plot in terms of the molar ratios of $Al_2O_3/(Na_2O+K_2O)$ and $Al_2O_3/(CaO+Na_2O+K_2O)$, the Cida granites and nordmarkites are peralkaline, metaluminous to peraluminous, and the Ailanghe granites are peraluminous (Fig. 3b). Notably, most samples from the Cida pluton which contain evidence of original peralkaline ferromagnesian minerals (e.g., riebeckite) plot as metaluminous to peraluminous. The discrepancy between primary mineral assemblage and major-element composition correlates directly with the extent of deuteric alteration. Such alteration typically results in chemical breakdown of primary ferromagnesian mineral assemblages and thus whole-rock compositions are modified toward apparent peraluminosity (Tollo et al., 2004). However, almost all the samples have $Al_2O_3/(CaO+Na_2O+K_2O)$ (alumina saturation index) less than 1.1, suggesting that they belong to A-type and/or I-type granites, according to the criteria of Chappell and White (1992). All rocks of the Cida and Ailanghe plutons display regular trend of decreasing FeO*, MgO, CaO and Al_2O_3 with increasing SiO_2. The Ailanghe granites have lower FeO* and Na_2O, and higher K_2O abundances at given SiO_2 (Fig. 4).

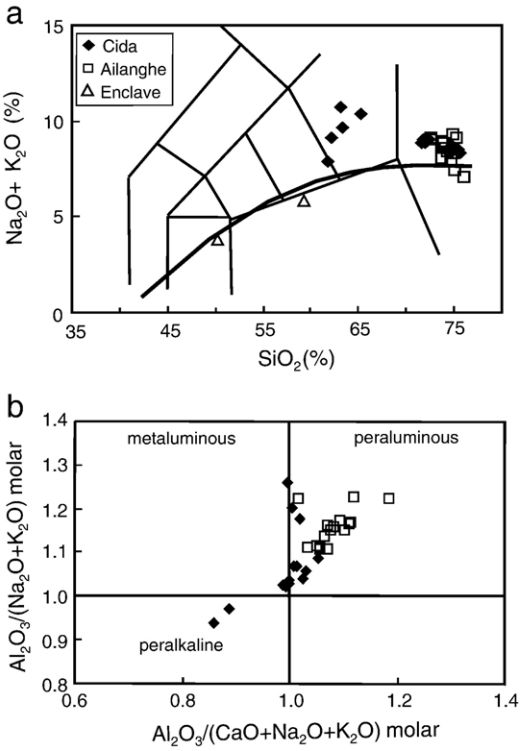

Fig. 3. (a) Chemical composition of the Cida granitoids, enclaves and Ailanghe granitic rocks plotted in the TAS classification diagram of Le Maitre et al. (1989). The bold solid line separates subalkaline and alkaline compositions; (b) Chemical composition of the Cida and Ailanghe granitic rocks in terms of alumina saturation. The major element data of the Cida granitoids are from Table 2, and those of the Ailanghe granites are from Table 2 and Cong (1988).

For the Cida granitoid suite, strontium and Ba generally decrease with increasing SiO_2, whereas Zr is extremely enriched (up to 1650 ppm) and an inflection at 72% SiO_2 marks a change in trend from enrichment to depletion. Rb shows little correlation with increasing silica (Fig. 5). The Cida granitoids share all the features common to A-type granitic rocks in terms of trace element geochemistry. They are typically enriched in Ga, Zr, Nb and Y, and depleted in Ba and Sr (Collins et al., 1982; Whalen et al., 1987) (Table 2; Figs. 5 and 6a). These rocks display similar patterns in a primitive-mantle-normalized spidergram, with the characteristic negative anomalies in Ba, Sr, Eu and Ti (Fig. 6a). The Cida nordmarkites are compositionally more diverse than the Cida granites, since they merely occur as marginal facies. Three nordmarkite samples (CD0404, CD0405 and CD0406) have elevated contents of CaO (2.2–3.2%), MgO (0.8–1.9%) and abnormally high abundances of Ba (255–535 ppm) and Sr (92–162 ppm). Judging from the presence of salite grains rimmed by ribeckite, we suggest that these nordmarkites contain cumulus phase (e.g., salite and alkali-feldspar). The other two nordmarkite samples (CDG0502 and CDG0508) have comparatively low CaO (1.5–1.6%), MgO (0.17–0.26%) contents and very low Ba (38–79 ppm) and Sr (6.7–8.5 ppm) concentrations, which are the result of extensive plagioclase and/or K-feldspar fractionation. However, the proportion of cumulus crystals is small causing only Ba and lesser Sr enrichment, as all the nordmarkite samples have similar REE abundances. The gabbroic and dioritic enclave samples (BMG0501 and BMG0502) exhibit similar patterns except that the gabbroic enclave lacks Ba and Sr depletion (Fig. 6a). In contrast, the Ailanghe granites have much lower Ga, Zr, Nb and Y, and much higher Ba and Sr concentrations relative to those of the Cida granitoids (Table 2; Figs. 5 and 6). In the spidergram, the Ailanghe granites show significant depletion in Ba, Nb, Ta, Sr, and Ti and slight enrichment in Pb (Fig. 6b).

Rare earth elements (REE) are enriched in the Cida granitoids relative to the Ailanghe granites. The

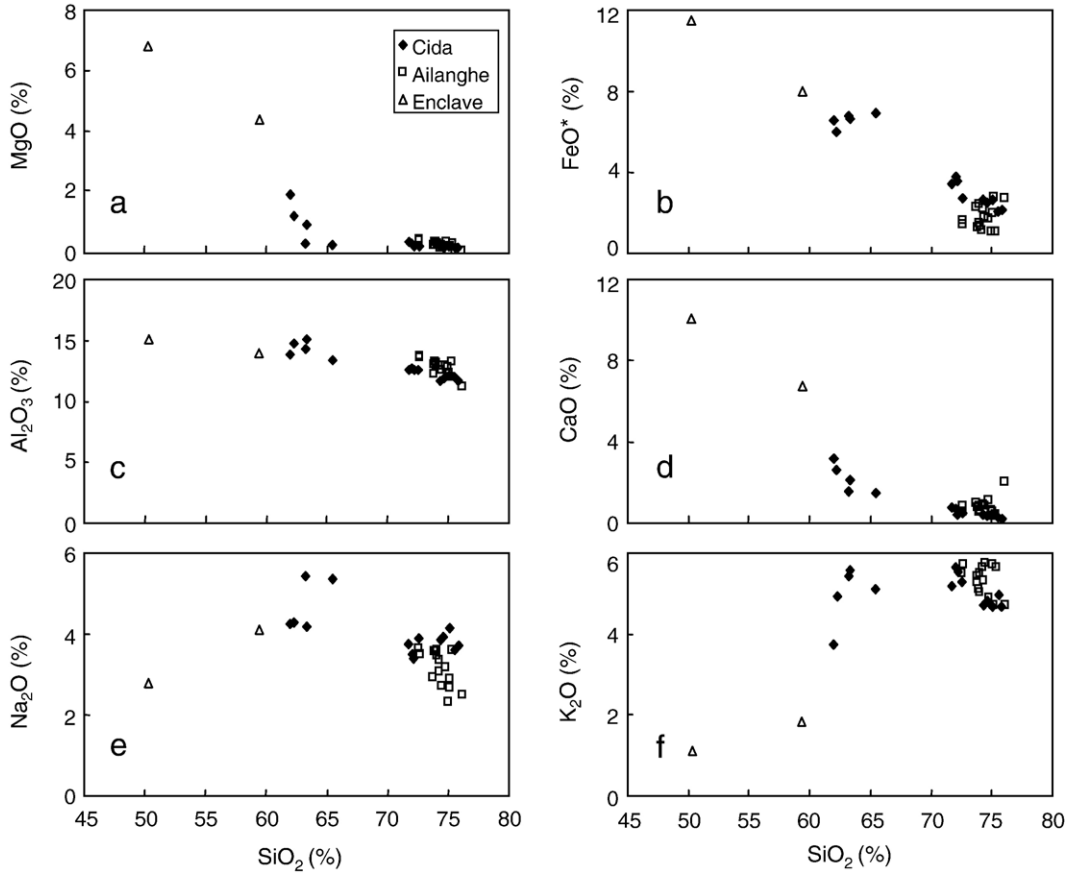

Fig. 4. Selected variation diagrams of major element oxides and silica for the Cida granitoids, enclaves and Ailanghe granitic rocks. The data are from the same source as those in Fig. 3.

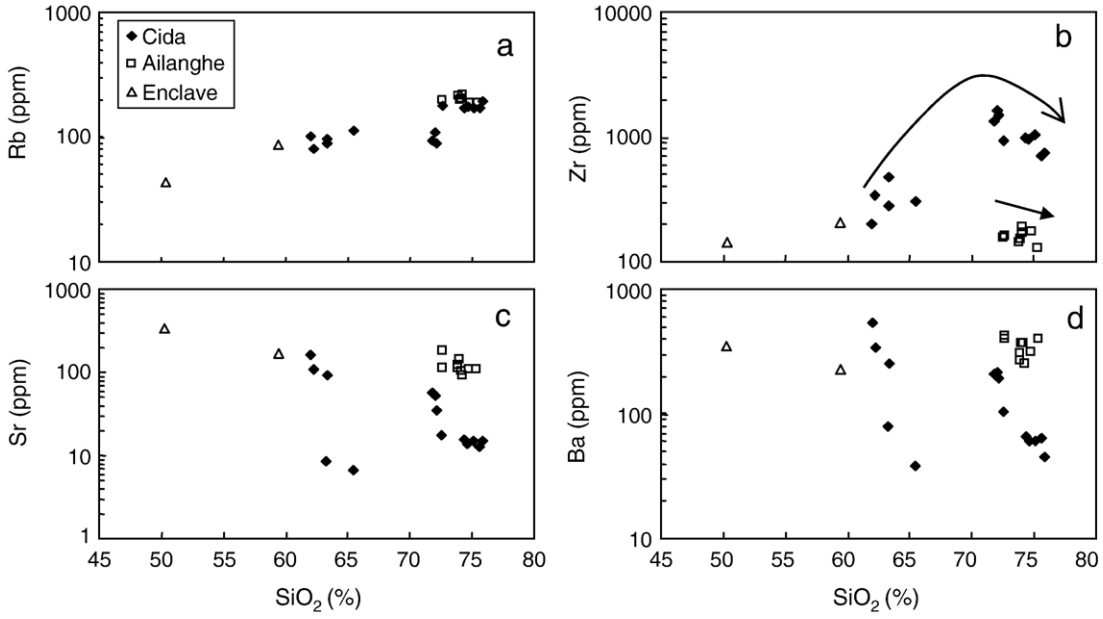

Fig. 5. Selected variation diagrams of trace elements and silica for the Cida granitoids, enclaves and Ailanghe granitic rocks.

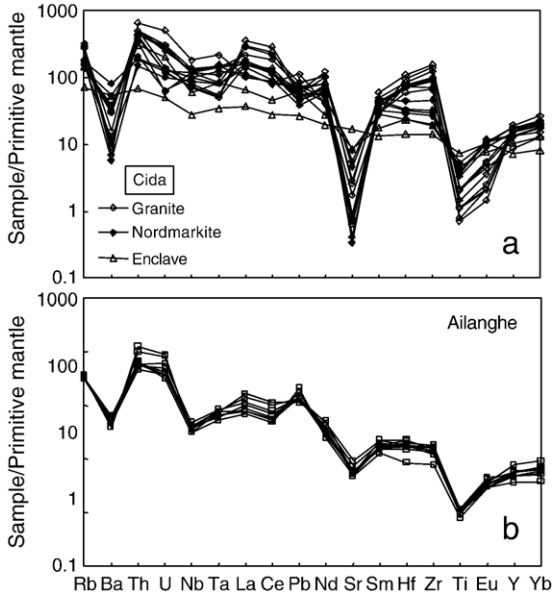

Fig. 6. Primitive mantle-normalized incompatible element distribution spidergrams for the (a) Cida granitoids, enclaves and (b) Ailanghe granitic rocks. The normalization values are from McDonough and Sun (1995).

chondrite-normalized REE diagram (Fig. 7a) for the Cida granitoids shows large variations in REE abundances among the different samples. They exhibit extreme negative Eu anomalies (δEu = 0.06 − 0.46), moderate light REE (LREE) enrichment (La_N/Sm_N = 3.5–6.2), and nearly flat heavy REE (HREE) distributions (Gd_N/Yb_N = 1.0–2.2). The chondrite-normalized REE patterns (Fig. 7b) of the Ailanghe granites resemble those of the Cida samples, but the Ailanghe granites show more pronounced enrichment in the LREE relative to HREE (La_N/Yb_N = 10.8–31.9), slightly greater LREE fractionation (La_N/Sm_N = 5.0–7.2), and similar negative Eu anomalies (δEu = 0.19 − 0.32).

The 10,000 × Ga/Al ratios of the Cida granitoids range from 3.36 to 4.29, similar to the global average of 3.75 for A-type granites (Whalen et al., 1987). In contrast, the 10,000 × Ga/Al ratios of the Ailanghe granites are much lower (1.78–2.36). In a Ga/Al versus Zr diagram (Fig. 8a), the Cida granitoids are all classified as A-type granite, whereas the Ailanghe granites fall in the field for I and S-type granites. Combined with the characteristic alumina saturation index (<1.1) (Chappell and White, 1992), the Ailanghe granites belong to I-type granite.

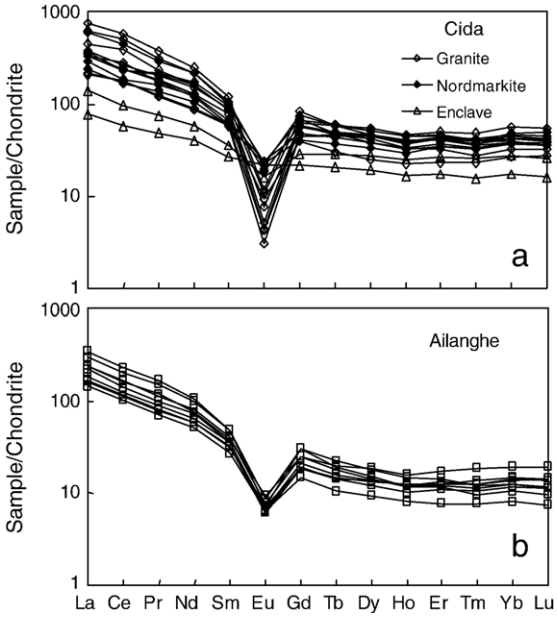

Fig. 7. Chondrite-normalized REE diagrams for the (a) Cida granitoids, enclaves and (b) Ailanghe granitic rocks. The normalization values are from Boynton (1984).

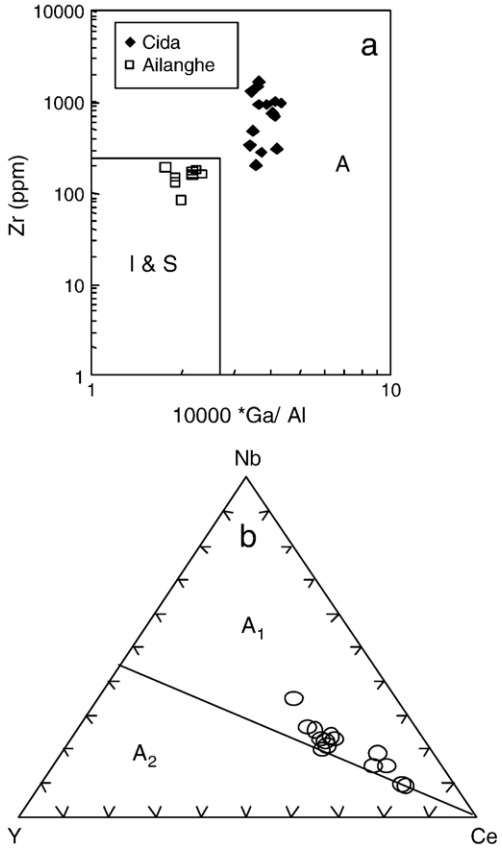

Fig. 8. Plots of the Cida and Ailanghe granitic rocks in (a) Zr vs. 10,000 × Ga/Al diagram of Whalen et al. (1987) showing affinity of A-type granites; (b) Nb–Y–Ce ternary diagram for the subdivision of A_1- and A_2-type granites (Eby, 1992). Only the Cida granitic rocks are plotted in b.

Furthermore, the Cida granitoids correspond to the A_1-group of Eby (1992), consistent with their anorogenic setting (Fig. 8b).

5.3. Nd–Sr isotopes

Nd and Sr isotopic data have been obtained from the representative Cida and Ailanghe samples (Table 3). The Cida A-type granitoids display very uniform initial ε_{Nd} values ranging from −0.25 to 0.24 and a relatively large variation in $(^{87}Sr/^{86}Sr)_i$ ratios from 0.7023 to 0.7053 (Fig. 9a), indicating a major mantle component in their genesis. The gabbroic and dioritic enclaves in the Cida pluton have $\varepsilon_{Nd}(t)=0.55–1.35$ and $(^{87}Sr/^{86}Sr)_i=0.7051–0.7053$, which are identical to those of the Cida granitoids. Notably, the initial Sr isotopic ratio for the sample CD0402 is relatively lower because of high Rb/Sr ratio and the true value is more probably somewhat higher. The Nd–Sr compositions of the Cida ganitoids are comparable with those of the contemporaneous Emeishan flood basalts and mafic intrusions (Xu et al., 2001; Zhong et al., 2003; Xiao et al., 2004; Zhong et al., 2004). The Ailanghe I-type granites have much lower $\varepsilon_{Nd}(t)$ ratios (−6.34 to −6.26) but much higher $(^{87}Sr/^{86}Sr)_i$ values (0.7102 to 0.7111), suggesting considerable contribution of ancient crustal component in the petrogenesis of these granites.

Sm–Nd model ages provide useful information about the age of the protolith and the petrogenesis of granitic magma. The Cida and Ailanghe samples have much lower values of $f_{Sm/Nd}$ (−0.45 to −0.56) than that of the continental crust (−0.40) (e.g., Jahn and Condie, 1995), and are likely produced by extensive fractional crystallization involving high Sm/Nd accessory minerals, such as apatite, titanite and hornblende. To minimize this effect, a two-stage Nd model age (T_{2DM}) is calculated using the same formulation as Keto and Jacobsen (1987). The Cida and Ailanghe granitic rocks show a very limited range of T_{2DM} model ages, respectively, but the latter have distinctly older T_{2DM} than the former.

6. Discussion

6.1. Petrogenesis

The data presented above show that the Cida granitoids are typically of A-type granites whereas the Ailanghe granites are discriminated as I-type granites. On the basis of SHRIMP zircon analyses, the emplacement age of the Cida A-type granitoids is ~261 Ma, coeval with that of the associated Baima mafic layered

Table 3
Sr and Nd isotopic data for the Cida and Ailanghe granitic rocks

Sample no.	Rb* (ppm)	Sr* (ppm)	$^{87}Rb/^{86}Sr$*	$^{87}Sr/^{86}Sr$	Error (2σ)	$(^{87}Sr/^{86}Sr)_i$	Sm* (ppm)	Nd * (ppm)	$^{147}Sm/^{144}Nd$*	$^{143}Nd/^{144}Nd$	Error (2σ)	$\varepsilon_{Nd}(t)$	T_{DM} (Ga)	T_{2DM} (Ga)	$f_{Sm/Nd}$
CD-0401	94.2	56.9	4.7914	0.722188	±15	0.704466	19.7	128	0.0921	0.512469	±12	0.18	0.85	1.01	−0.53
CD-0402	108	52.6	5.9637	0.724310	±10	0.702251	23.6	152	0.0931	0.512463	±13	0.03	0.87	1.03	−0.53
CD-0403	89.1	34.6	7.4613	0.732708	±10	0.705110	11.6	71.6	0.0971	0.512468	±11	−0.01	0.89	1.03	−0.51
CD-0404	89.9	92.0	2.8247	0.715277	±10	0.704829	20.0	129	0.0932	0.512473	±13	0.22	0.86	1.01	−0.53
CD-0405	79.6	108	2.1254	0.712410	±12	0.704548	18.6	103	0.1089	0.512501	±12	0.24	0.94	1.01	−0.45
CD-0406	102	162	1.8220	0.712019	±14	0.705280	11.4	62.9	0.1090	0.512476	±10	−0.25	0.98	1.05	−0.45
BMG-0501	42.8	340	0.3646	0.706414	±13	0.705065	5.32	24.2	0.1326	0.512598	±9	1.35	1.04	0.92	−0.33
BMG-0502	86.5	168	1.4867	0.710766	±12	0.705267	7.03	34.7	0.1219	0.512539	±12	0.55	1.01	0.98	−0.38
ALH-0401	190	110	5.0089	0.728741	±9	0.710214	9.29	64.5	0.0867	0.512128	±11	−6.30	1.23	1.55	−0.56
ALH-0402	198	112	5.1262	0.730054	±12	0.711093	7.45	46.1	0.0973	0.512148	±12	−6.26	1.31	1.54	−0.51
ALH-0403	196	184	3.0829	0.721794	±12	0.710391	9.37	58.3	0.0967	0.512143	±12	−6.34	1.31	1.55	−0.51

Note: All the initial isotopic ratios were corrected to 260 Ma. *: $^{87}Rb/^{86}Sr$ and $^{147}Sm/^{144}Nd$ were calculated from Rb, Sr, Sm and Nd abundances determined by ICP-MS. The details for single-(T_{DM}) or two-stage (T_{2DM}) model age calculations are given by Jahn et al. (1999).

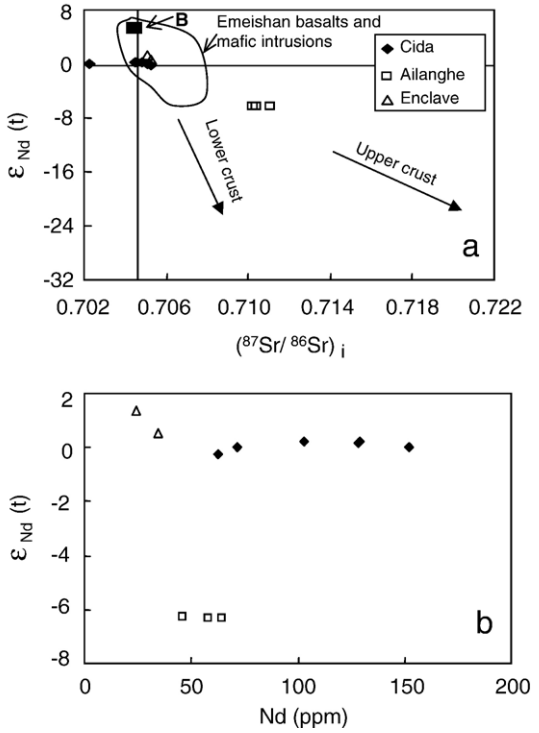

Fig. 9. (a) $\varepsilon_{Nd}(t)$ vs. $(^{87}Sr/^{86}Sr)_i$ diagram for the Cida granitoids, enclaves and Ailanghe granitic rocks. B=Emeishan basalts (Xu et al., 2001). The data of the mafic intrusions and Emeishan basalts are from Xu et al. (2001), Zhong et al. (2003, 2004), Xiao et al. (2004). The trends to the lower and upper crust are similar to those of Jahn et al. (1999); (b) Nd vs. $\varepsilon_{Nd}(t)$ diagram for the Cida granitoids, enclaves and Ailanghe granitic rocks.

intrusion (SHRIMP zircon age of 262±2 Ma; Zhou et al., 2005). In contrast, the Ailanghe granite has a crystallization age of ~251 Ma, younger than that of the associated mafic/ultramafic Hongge layered intrusion (259.3±1.3 Ma; Zhong and Zhu, 2006). Thus, the emplacement age of the Cida granitic pluton is older than that of the Ailanghe granites.

The petrogenesis and tectonic significance of A-type granites remain controversial. Numerous petrogenetic models have been proposed for the origin of A-type granits, mainly including (1) fractionation of mantle-derived magmas with or without interaction with crustal rocks (Loiselle and Wones, 1979; Eby, 1990; Turner et al., 1992; Kerr and Fryer, 1993; Han et al., 1997); (2) low degrees of melting of residual granulites (Collins et al., 1982; Clemens et al., 1986; Whalen et al., 1987); (3) anatexis of underplated tonalitic I-type granites to tholeiites and their differentiates (Anderson, 1983; Sylvester, 1989; Creaser et al., 1991; Skjerlie and Johnston, 1992; Patiño Douce, 1997; Frost and Frost, 1997; Frost et al., 2001; Wu et al., 2002); (4) melting of lower-crustal source rocks under fluxing of mantle-derived volatiles or metasomatism of granitic magmas (Bailey, 1978; Taylor et al., 1980; Harris et al., 1986). Therefore, the key issues concerning A-type granitoids origin are the role of mantle-derived material and its interaction with lower to middle continental crust, as will be discussed below regarding the Cida and Ailanghe granitic suites.

6.1.1. Fractional crystallization

The Cida A-type granitoids and Ailanghe I-type granites are distinct, but a general fractional crystallization

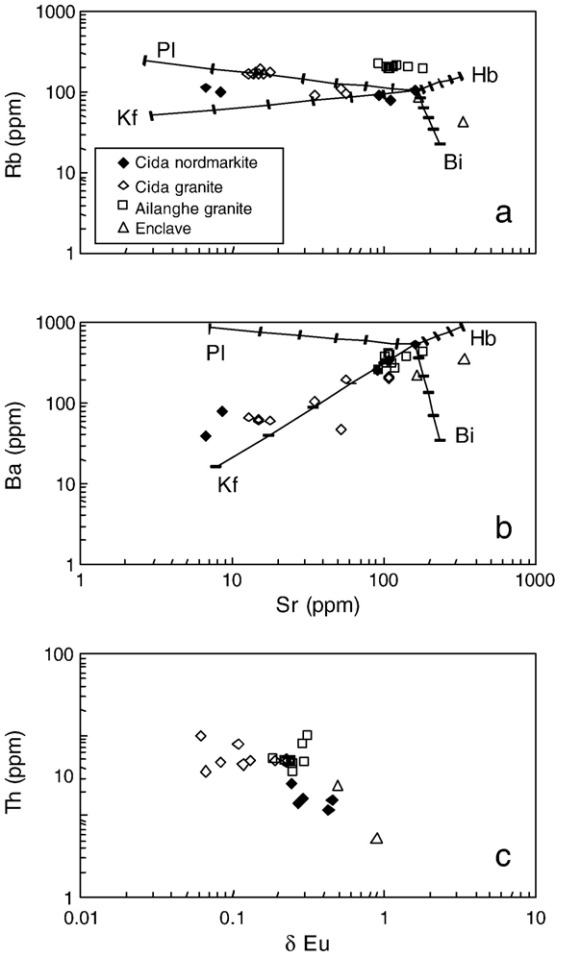

Fig. 10. Plots of (a) Rb vs. Sr, and (b) Ba vs. Sr, and (c) Th vs. δEu for the Cida granitoids, enclaves and Ailanghe granitic rocks. Mineral fractionation vectors calculated using partition coefficients from Nash and Crecraft (1985) for biotite and K-feldspar, and Bacon and Druitt (1988) for hornblende and plagioclase, except Mahood and Hildreth (1983) for Ba in biotite and Arth (1976) for Ba in K-feldspar. The composition of the least evolved nordmarkite sample (CD0406) is assumed to represent the initial melt composition of the Cida granitoids. Tick marks indicate percentage of mineral phase removed, in 10% intervals.

trend is illustrated by decreasing MgO, FeO*, Al_2O_3, CaO, Na_2O, Sr, and Ba contents with increasing SiO_2 (Figs. 4 and 5). The Cida and Ailanghe granitic suites are characterized by the very low MgO contents (Table 2), which is interpreted as due to the fractionation of Mg-rich minerals such as olivine, clinopyroxene and hornblende. These minerals are abundant in the temporally and spatially associated Baima and Hongge mafic/ultramafic intrusions. From the REE patterns, hornblende may be considered as an important phase fractionated from magmas, because it is able to produce a concave HREE pattern without significant HREE fractionation in intermediate and acidic magmas (Martin et al., 1994; Han et al., 1997). Significant degrees of fractional crystallization have occurred during the formation of the Cida granitoids and Ailanghe granites. This is clearly indicated by the striking depletions in Ba, Sr, Ti, and Eu as shown in the spidergrams (Fig. 6) and REE patterns (Fig. 7). Negative Ti anomaly is commonly related to ilmenite or titanite fractionation.

In granitic systems, the feldspar would be the most important minerals in any fractional crystallization scheme, and the size of the negative Eu anomaly would be a measure of the degree of feldspar fractionation. Large negative Eu depletion in the Cida and Ailanghe samples requires extensive fractionation of feldspars, while the negative Eu anomaly is much pronounced in the Cida A-type granites than in the Ailanghe I-type granites (Table 2; Fig. 7). Fig. 10a and b indicate that fractionation of feldspar may have resulted in a small increase in Rb but a considerable decrease in Sr and Ba for the Cida granitoids. The calculated effects of fractional crystallization from the least evolved nordmarkite sample (CD0406) are shown in mineral vector diagrams on Fig. 10 and b. The Cida granitoids display a combined vector of potassium feldspar and plagioclase fractionation in Fig. 10a, suggesting that both plagioclase and potassium feldspar have played the same significant role during the magmatic differentiation. Fig. 10b shows that potassium feldspar fractionation was more important than plagioclase in controlling Ba abundances. Compositional trend of the Cida nordmarkite and granite indicate fractionation of up to 40–50 wt.% of K-feldspar and plagioclase. In addition, there is a regular trend of increasing enrichment in Th with an increase in the size of negative Eu anomaly for the Cida granitoids (Fig. 10c). The fractionation models of Rb, Sr and Ba therefore suggest that the Cida nordmarkite and granite are consanguineous and extensive fractional crystallization can lead to residual magma having trace elements abundances typical of A-type granitoids. In contrast, the evolution of the Ailanghe suite was largely controlled by plagioclase fractionation as shown in Fig. 10.

As shown above, the Cida A-type granitoids are characterized by much higher Zr, Nb, Ga contents and Rb/Sr ratios, significantly lower Ba, Th, U contents and LREE/HREE ratios than the Ailanghe I-type granites. It has been suggested that potentially sensitive incompatible-element ratios (e.g., Th/U, Rb/U, Rb/Pb) could reveal systematic differences between different granitic plutons, although they are quite variable, especially at high SiO_2 (Kerr and Fryer, 1993). The difference of Th/U ratios for the Cida (5.0–21) and Ailanghe (3.9–7.7) plutons indicate they were differently generated, and the Cida granitic rocks could be closely related to the more mafic magma due to their higher Th/U ratios. Furthermore, the difference between crustal contamination and crystal fractionation is well expressed in diagrams using trace element ratios such as Nb/Y and Rb/Y (Fig. 11). In such diagrams, crustal compositions and crustal melts are distinguished by high Rb/Nb ratios. The Cida granitic rocks have low Rb/Nb ratios (1.2–2.3), which are comparable to those of the Emeishan basalts (0.3–1.9; except one sample; Xu et al., 2001; Zhong et al., 2006) in the Pan-Xi area. In contrast, the Ailanghe granites have much higher Rb/Nb ratios (6.5–10.8) and plot close to middle crust values (Rudnick and Fountain, 1995). Thus, it would appear that there was predominant crystal fractionation in the Cida granitoids. Conversely, crystal fractionation plus crustal components dominated in the Ailanghe granites.

A chemical trend that Zr increases then decreases with increasing SiO_2 is displayed in the Cida granitic suite (Fig. 5b). This indicates that zircon was not

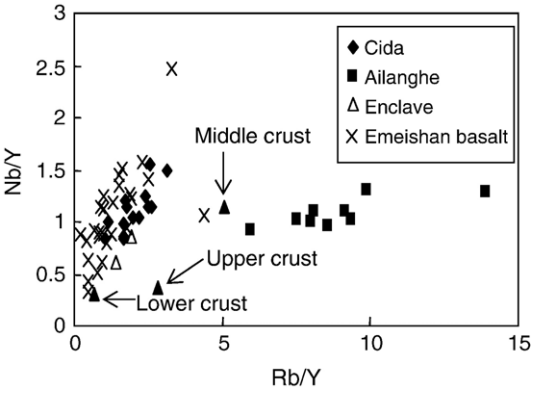

Fig. 11. Nb/Y vs. Rb/Y diagram for the Cida granitoids, enclaves and Ailanghe granitic rocks compared to the Emeishan basalts in the Pan-Xi area (Xu et al., 2001; Zhong et al., 2006). The lower and middle crustal compositions are from Rudnick and Fountain (1995), and the upper crustal compositions are from Taylor and McLennan (1985).

saturated in the nordmarkites but saturated in the granites, which was also controlled by fractional crystallization. In contrast, the Ailanghe granites exhibit continuously decreasing Zr with increasing SiO_2 (Fig. 5b), consistent with zircon separation from the evolving melt. Zircon saturation thermometry (Watson and Harrison, 1983) provides a simple and robust means of estimating magma temperatures from bulk-rock compositions. The calculated zircon saturation temperatures (T_{Zr}) of the Cida felsic rocks are 993–1100 °C, whereas T_{Zr} of the Ailanghe granites range from 771 to 847 °C (Table 2). T_{Zr} of the least fractionated granite could approximately represent a primary unfractionated (zircon unsaturated) melt composition. The distinct origin of the Cida A-type granitoids is therefore also shown by their much higher values of zircon saturation temperatures (T_{Zr}) relative to the Ailanghe I-type granites.

6.1.2. Nature of the sources and the role of crustal sources

The Nd, Sr isotopic data and T_{2DM} model ages (Table 3; Fig. 9) suggest that different sources contributed to the chemistry of the Cida and Ailanghe granitic suites, consistent with the observations of the trace element compositions. The similarity in Nd–Sr isotopic distributions of the Cida A-type granitoids to those of the Emeishan basalts implies that they share a common source. Furthermore, $\varepsilon_{Nd}(t)$ values of the coeval and spatially associated Baima gabbros range from 1.13 to 1.62 (Zhang et al., 1999), which are similar to those of the coeval Hongge mafic/ultramafic intrusion ($\varepsilon_{Nd}(t)=-2.68$ to 1.02) (Zhong et al., 2003). It is thus suggested that the Cida granitic rocks and the mafic rocks in the ELIP are both generated by a mantle plume starting at the base of the Yangtze craton (Chung and Jahn, 1995; Xu et al., 2001).

In contrast, the Ailanghe I-type granites have high initial $^{87}Sr/^{86}Sr$ ratios (0.7102–0.7111), negative $\varepsilon_{Nd}(t)$ values (−6.34 to −6.26), and much older Sm–Nd model ages (T_{2DM}=1.54–1.55 Ga), favoring a significant contribution from crustal material. The Ailanghe granites are characterized by marked negative Nb and Ta anomalies and slightly positive Pb anomalies in the spidergram (Fig. 6b), which is also consistent with involvement of crustal compositions (Rudnick and Fountain, 1995). Combined studies of $^{87}Sr/^{86}Sr$, $^{143}Nd/^{144}Nd$ (Fig. 9a) and the trace element ratios (Fig. 11) indicate that the middle–upper crust but not the lower crustal component involved in the generation of the Ailanghe granites. The peraluminous, silica-rich composition of the Ailanghe granites suggests an important contribution of metasedimentary material in their source. From an extensive compilation of Sm–Nd isotopic compositions and T_{DM} values for intrusive granitoids, sedimentary and metamorphic rocks, Chen and Jahn (1998) demonstrated that the Yangtze–Cathaysia craton is essentially made up of Proterozoic rocks. The correlation between T_{DM} of igneous intrusions and basement rocks in SE China suggests that Proterozoic basement rocks have played a key role in petrogenesis of both I- and S-type igneous rocks. The Ailanghe granites with the Sm–Nd model ages (T_{2DM}) of 1.54–1.55 Ga, were emplaced in the upper part of the Paleo-Mesoproterozoic Huili Group. The Huili Group or its equivalents, the Kunyang and Yanbian Groups, which consists of low-grade metasedimentary rocks interbedded with felsic and mafic metavolcanic rocks (SBGMR, 1991), are widely distributed in the inner zone of the ELIP (Xu et al., 2004). The Hekou Formation, which is the lowermost part of the Huili Group, consists mainly of schists, albitite, slates, and meta-sandstones. These rocks have been suggested to be of volcanic-sedimentary origin (SBGMR, 1991). Palaeoozoic and Early Mesozoic granitoids in SE China were believed to be produced by remelting of Paleo- to Mesoproterozoic crustal rocks (Chen and Jahn, 1998). The lack of correlation between $\varepsilon_{Nd}(t)$ values and Nd concentrations for the Ailanghe granites (Fig. 9b) precludes assimilation and fractional crystallization (AFC) as major processes during their late evolutionary stages at shallow crustal level. This could imply that the Ailanghe granites were probably derived from partial melting of Paleo-Mesoproterozoic metamorphic rocks from the Huili Group at depth, although we do not know exactly its isotopic characteristics.

6.1.3. Petrogenetic models

Geochemical and isotopic data suggest that the Cida A-type granitoids and Ailanghe I-type granites are highly fractionated granitic rocks. Their distinct features demand a different origin. Petrogenetic models to explain the generation of felsic magmas fall into two broad categories (Riley et al., 2001). The first is where felsic magmas are derived from a mafic parent magma by fractional crystallization or assimilation combined with fractional crystallization (AFC). This process is often suggested for small magma batches, because to generate large volumes of felsic magma, unreasonably large amounts of basalt must be crystallized. The second model, in which mafic magmas provide heat for the partial melting of crustal rocks, is considered more appropriate for large volume felsic magma bodies.

A model involving fractional crystallization from a basaltic parent (e.g., Loiselle and Wones, 1979; Turner

et al., 1992; Peccerillo et al., 2003) provides the most satisfactory explanation for the geochemistry of the Cida A-type granitoids. The Cida granitoids have Nd–Sr isotopic signatures largely overlapping with the associated and contemporaneous Baima mafic intrusion (~260 Ma) and the other mafic intrusive and extrusive rocks in the Pan-Xi area, favoring its derivation from basaltic magmas. Furthermore, the presence of mafic and intermediate enclaves and synplutonic mafic dikes within the Cida stock indicate that basaltic magmas were coeval with the granites. Significant fractionation from a basaltic parent is strongly supported by depletion of compatible elements occurred along with enrichment of incompatible elements and extreme depletion in Sr and Eu produced by removal of abundant plagioclase. In addition, the amount of basaltic magmas added to the continental crust was much greater than the volume of A-type granite for the Cida case, indicating that fractional crystallization is a reasonable model because only small amounts of granitic magma can be generated from mafic rocks either by partial melting or by extensive fractional crystallization (Wager and Brown, 1968). A scenario involving remelting of underplated mafic rocks, recently extracted from the mantle, is also an alternative to pure fractional crystallization of mantle melts. It has been suggested that models of incompatible vs compatible trace elements are potentially powerful tools to discriminate between fractional crystallization and melting processes (Peccerillo et al., 2003). Geochemical modeling shows that the Zr against Sr and V variations cannot be obtained by a single-stage partial melting of mafic rocks (Fig. 12). In contrast, the overall Sr and V vs Zr variation in the Cida granites can be obtained by fractional crystallization starting from the mafic enclave (BMG0501). In part, the enrichment levels of some Zr are higher than Rayleigh fractionation can be attributed to enrichment in a residual melt phase. Thus, the Cida granitic suite is interpreted as having a direct derivation from mantle sources via extended fractional crystallization of basaltic parental magmas.

However, the general lack of intermediate compositions has been raised in objection to the fractionation model for A-type granites. A petrological, geochemical and thermodynamic modeling study has recently been reported for the basalts and silicic peralkaline rocks from the Quaternary Gedemsa volcano, northern Ethiopian rift. It suggests that, with a steady fall in temperature, fractionating magmas pass rapidly through the intermediate stages, i.e., producing relatively small amounts of intermediate melts (Peccerillo et al., 2003). This is expected, as contemporaneous separation of various minerals occurs over a narrow temperature interval

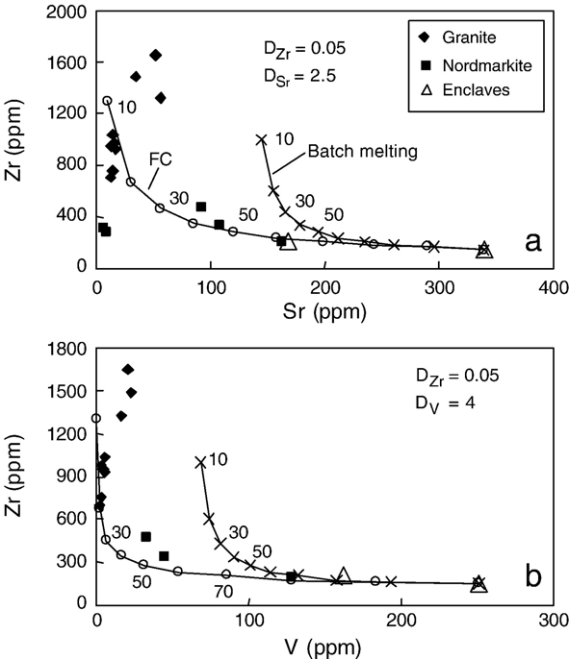

Fig. 12. Variation diagram with batch melting and fractional crystallization (FC) models of compatible vs. incompatible trace elements for the Cida granitic rocks. The gabbroic enclave sample (BMG0501) is assumed as the starting composition for both batch melting and fractional crystallization. Partition coefficients are similar to those of Peccerillo et al. (2003).

(Clague, 1978). Therefore, the mechanism of fractional crystallization effectively reduces the volume of intermediate melts. Moreover, in a fractionating, continuously fed magma chamber, the silicic melts will occupy the top of the reservoir and the mafic magmas pond at the bottom, whereas minor intermediate melts, rich in crystals, form the interface between the two zones (Wolff and Storey, 1984; Turner and Campbell, 1986). The silicic material sitting at the top of the chambers was preferentially emplaced into the crust to form A-type granites, whereas part of mafic material was left at depth and crystallized to give rise to mafic and ultramafic cumulate rocks. The apparent compositional gap during fractional crystallization is also evident in numerical simulation of silicic magma generation by basalt crystallization by Annen and Sparks (2002). Their study suggests that in almost all cases silicic melts generated by differentiation of basalt are significant contributions to melt generation. A seismic tomographic modeling shows that the lower crust in the inner zone of the ELIP has a high seismic P-wave velocity ranging from 7.1 to 7.8 km/s (Liu et al., 2001). The high V_p body might represent the residues left after extensive melt extraction from the plume head (Xu et al., 2004). Thus, the Cida granitoids could be produced by extensive fractional

crystallization of mantle-derived basaltic parents, as are high temperatures estimated for Cida magmas (up to 1100 °C).

In contrast, the peraluminous, silica-rich composition and isotope data of the Ailanghe granite pluton (Table 2; Figs. 3b, 9a) would be explained by partial melting of the middle to upper crustal metasedimentary and metavolcanic rocks from the Paleo-Mesoproterozoic Huili Group. The high heat required for partial melting of the crustal rocks can be provided by the upwelling of the Emeishan mantle plume. Notably, seismic refraction experiments have identified a high-velocity layer (6.9 to 7.0 km/s) in the lower crust beneath the Hongge area (Zhang et al., 1988), implying the presence of the underplated basalts and their differentiated equivalents. The emplacement age of the Ailanghe granites is slightly younger than the associated Hongge mafic/ultramafic intrusion and the main eruption age of the Emeishan basalts at ~260 Ma (Ali et al., 2002; Zhou et al., 2002; Courtillot and Renne, 2003; Zhong and Zhu, 2006). Addition of basaltic material in the source may also contribute to the generation of the Ailanghe granites, although it is very difficult to determine its proportion due to lack of the isotopic component in potential crustal source rocks. Thus, the Ailanghe I-type granites were probably formed by partial melting of the pre-existing old middle–upper crust and newly underplated basaltic component. The magmas parental to the Ailanghe granites would further experience extensive magmatic differentiation to account for their geochemical features as shown above.

6.2. Tectonic significance

The Permian Emeishan large igneous province (ELIP), consisting of massive flood basalts, numerous ultramafic/mafic intrusive rocks, granites, and syenites, has recently been believed to originate from a mantle plume (e.g., Chung and Jahn, 1995; Chung et al., 1998; Xu et al., 2001; Song et al., 2001; He et al., 2003; Xu et al., 2004). The SHRIMP U–Pb dating results lead us to conclude that emplacement of the A-type and I-type granites took place in a short interval between ~261 and 251 Ma (with errors in the range of ±6–4 Ma). Combined with the ages of the mafic rocks (Zhou et al., 2002; Lo et al., 2002; Zhong and Zhu, 2006), we consider that the granitic plutons formed coeval with or a few million years after the Emeishan trap magmatism.

The Cida and Ailanghe granitoids represent anorogenic magmatism (Fig. 8b) associated with mantle plume activity and they show the chemical characteristics considered diagnostic of A-type and I-type granites, respectively (Fig. 8a). The two granitic suites had distinct sources and generating mechanism. The generation of the granites in the ELIP was related to massive underplating of mafic magma and associated extensive partial melting. It is thus concluded that many compositional and genetically different types of granites can be produced in the same tectonic setting and their ultimate nature depends more importantly on the type and proportion of mantle and crustal material involved and melting conditions.

It has been proposed that mantle plumes are perhaps important for the lower continental crust (Condie, 1997). The plumes gave rise to juvenile crust either directly, by partial melting as they arrived at the base of the lithosphere, or indirectly by heating the upper mantle. Crustal growth by magmatic underplating may be a more important mechanism than is generally recognized (Frost et al., 2001). The crustal thickness in the inner zone of the ELIP ranges from 55 to 64 km (average 61.5 km), which is considerably thicker than that beneath eastern China (Zhang et al., 1988; Yuan, 1996; Liu et al., 2001; Xu et al., 2004). Furthermore, the thickness of the high-velocity lower crust, which is generally absent outside the inner zone (Cui et al., 1987), is as much as 25 km (average 20 km). It therefore suggests that significant melt production and possible underplating and/or intrusion into the lower crust caused by the Emeishan plume (Xu et al., 2004), may play an important role in producing juvenile crust in the inner zone.

7. Conclusions

The geochronological, geochemical and Nd–Sr isotopic study presented here lead to the following conclusions:

(1) SHRIMP zircon U–Pb dating yields crystallization ages of 261±4 Ma and 251±6 Ma for the Cida granitoids and Ailanghe granites in the Pan-Xi area, southwestern China, respectively. These granitic plutons formed during a period of anorogenic magmatism in response the Emeishan mantle plume activity some 260 Ma ago.
(2) The Cida granitoids and Ailanghe granites have both experienced extensive fractional crystallization. However, the Cida granitic stock exhibits A-type geochemical characteristics whereas the Ailanghe granites are silica-rich, peraluminous I-type granites. The Cida granitoids are typically rich in HFSEs (high field strength elements), such as Zr, Nb, Y, REE and Ga, but poor in Ba and Sr.

In contrast, the Ailanghe granites have relatively low contents of Zr, Nb, Y, HREE and Ga, and elevated contents of Ba and Sr.

(3) Geochemical, isotopic data and geochemical modeling suggest that the Cida and Ailanghe granitic rocks originate from contrasting source material. The Cida granitoids were produced by extensive fractional crystallization from a basaltic parent. The scarcity or absence of intermediate magmas is believed to derive essentially from the narrow temperature interval over which intermediate melts formed, a process that significantly reduces the amount of intermediate magmas. The high $(^{87}Sr/^{86}Sr)_i$ ratios and negative $\varepsilon_{Nd}(t)$ values and prominent negative mantle-normalized Nb and Ta anomalies and slightly positive Pb anomalies of the Ailanghe granites indicate their derivation from partial melting of middle–upper crustal, Paleo-Mesoproterozoic metasedimentary–metavolcanic rocks from the Huili group and newly underplated, mantle-derived mafic rocks.

(4) The formation of the granites in the inner zone of the ELIP was related to the Emeishan mantle plume activity. High melt production and possible underplating and/or intrusion into the lower crust triggered by the Emeishan plume, may exert a significant role in the generation of the juvenile crust.

Acknowledgments

We appreciate the assistance of Drs. Dunyi Liu, Yusheng Wan, Zhiqing Yang, Yuruo Shi and Ms. Hua Tao in SHRIMP dating, Dr. Caixia Feng in major element analysis by XRF, Dr. Xianglin Tu and Ms. Yaping Wang and Jing Hu for trace element analysis by ICP-MS, Drs. Fuken Chen, and Chaofeng Li for Nd–Sr isotopes analysis by TIMS. Prof. Y.-F. Zheng is thanked for beneficial discussion on an early draft. The constructive reviews of Professors Fuyuan Wu, and Tony Kemp, and the Editor, Professor Roberta Rudnick are greatly appreciated. This study was jointly supported by the "CAS Hundred Talents" Foundation of the Chinese Academy of Sciences to HZ, the National Natural Science Foundation of China (40473025) and grant from the Knowledge-innovation Program of the Chinese Academy of Sciences (KZCX3-SW-125).

References

Ali, J.R., Thompson, G.M., Song, X.Y., Wang, Y., 2002. Emeishan basalts (SW China) and the 'end-Guadalupian' crisis: magneto-biostratigraphic constraints. J. Geol. Soc. 159, 21–29.

Ali, J.R., Thompson, G.M., Zhou, M.F., Song, X.Y., 2005. Emeishan large igneous province, SW China. Lithos 79, 475–489.

Anderson, J.L., 1983. Proterozoic anorogenic granite plutonism of North America. In: Medaris, L.G., Mickelson, D.M., Byers, C.W., Shanks, W.C. (Eds.), Proterozoic Geology. Geol. Soc. Am. Mem., vol. 161, pp. 133–154.

Annen, C., Sparks, R.S.J., 2002. Effects of repetitive emplacement of basaltic intrusions on thermal evolution and melt generation in the crust. Earth Planet. Sci. Lett. 203, 937–955.

Arth, J.G., 1976. Behaviour of trace elements during magmatic processes: a summary of theoretical models and their applications. J. Res. U. S. Geol. Surv. 4, 41–47.

Bacon, C.R., Druitt, T.H., 1988. Compositional evolution of the zoned calcalkaline magma chamber of Mount Mazama, Crater Lake, Oregon. Contrib. Mineral. Petrol. 98, 224–256.

Bailey, D.K., 1978. Continental rifting and mantle degassing. In: Neumann, E.R., Ramberg, I.B. (Eds.), Petrology and Geochemistry of Continental Rifts. Reidel, Dordrecht, pp. 1–13.

Black, L.P., Kamo, S.L., Allen, C.M., Aleinkoff, J.N., Davis, D.W., Korsch, R.J., Foudoulis, C., 2003. TEMORA 1: a new zircon standard for Phanerozoic U–Pb geochronology. Chem. Geol. 200, 155–170.

Boynton, W.V., 1984. Geochemistry of the rare earth elements: meteorite studies. In: Henderson, P. (Ed.), Rare Earth Element Geochemistry. Elsevier, pp. 63–114.

Chappell, B.W., White, A.J.R., 1992. I- and S-type granites in the Lachlan Fold Belt. Trans. R. Soc. Edinb. Earth Sci. 83, 1–26.

Chazot, G., Bertrand, H., 1995. Genesis of silicic magmas during Tertiary continental rifting in Yemen. Lithos 36, 69–83.

Chen, J.F., Jahn, B.M., 1998. Crustal evolution of southeastern China: Nd and Sr isotopic evidence. Tectonophysics 284, 101–133.

Chung, S.L., Jahn, B.M., 1995. Plume-lithosphere interaction in generation of the Emeishan flood basalts at the Permian–Triassic boundary. Geology 23, 889–892.

Chung, S.L., Jahn, B.M., Wu, G.Y., Lo, C.H., Cong, B.L., 1998. The Emeishan flood basalt in SW China: a mantle plume initiation model and its connection with continental break-up and mass extinction at the Permian–Triassic boundary. In: Flower, M.F.J., Chung, S.L., Lo, C.H., Lee, T.Y. (Eds.), Mantle Dynamics and Plate Interaction in East Asia. AGU Geodyn. Ser., vol. 27, pp. 47–58.

Clague, D.A., 1978. The oceanic basalt–trachyte association: an explanation of the Daly Gap. J. Geol. 86, 739–743.

Clemens, J.B., Holloway, J.R., White, A.J.R., 1986. Origin of an A-type granite: experimental constraints. Am. Mineral. 71, 317–324.

Collins, W.J., Beams, S.D., White, A.J.R., Chappell, B.W., 1982. Nature and origin of A-type granites with particular reference to southeast Australia. Contrib. Mineral. Petrol. 80, 189–200.

Compston, W., Williams, I.S., Kirschvink, J.L., Zhang, Z., Ma, G., 1992. Zircon U–Pb ages fro the Early Cambrian time-scale. J. Geol. Soc. Lond. 149, 171–184.

Condie, K.C., 1997. Contrasting sources for upper and lower continental crust: the greenstone connection. J. Geol. 105, 729–736.

Cong, B.L., 1988. Formation and Evolution of the Pan-Xi Paleorift. Science Press, Beijing. 424 pp. (in Chinese).

Courtillot, V., Renne, P.R., 2003. On the ages of flood basalt events. C. R. Geosci. 335, 113–140.

Courtillot, V., Besse, J., Vandamme, D., Montigny, R., Jaeger, J.J., Cappetta, H., 1986. Deccan flood basalts at the Cretaceous/Tertiary boundary? Earth Planet. Sci. Lett. 80, 361–374.

Creaser, R.A., Price, R.C., Wormald, R.J., 1991. A-type granites: assessment of a residual-source model. Geology 19, 163–166.

Cui, Z.Z., Luo, D.Y., Chen, J.P., Zhang, Z.Y., Huang, L.Y., 1987. Deep crust structure and tectonics in the Panxi area. Acta Geophys. Sin. 30, 566–579 (in Chinese).

Dobretsov, N.L., Vernikovsky, V.A., 2001. Mantle plumes and their geologic manifestations. Int. Geol. Rev. 43, 771–787.

Eby, G.N., 1990. The A-type granitoids: a review of their occurrence and chemical characteristics and speculations on their petrogenesis. Lithos 26, 115–134.

Eby, G.N., 1992. Chemical subdivision of the A-type granitoids: petrogenetic and tectonic implications. Geology 20, 641–644.

Fan, W.M., Wang, Y.J., Peng, T.P., Miao, L.C., Guo, F., 2004. Ar–Ar and U–Pb geochronology of the basalts in the western Guangxi province and constraints on the eruption ages of the Emeishan basalts. Chin. Sci. Bull. 49, 1892–1900.

Frindt, S., Trumbull, R.B., Romer, R.L., 2004. Petrogenesis of the Gross Spitzkoppe topaz granite, central western Namibia: a geochemical and Nd–Sr–Pb isotope study. Chem. Geol. 206, 43–71.

Frost, C.D., Frost, B.R., 1997. Reduced rapakivi-type granites: the tholeiite connection. Geology 25, 647–650.

Frost, C.D., Bell, J.M., Frost, B.R., Chamberiain, K.R., 2001. Crustal growth by magmatic underplating: isotopic evidence from the northern Sherman batholith. Geology 29, 515–518.

Govindaraju, G., 1994. Compilation of working values and sample description for 383 geostandards. Geostand. Newsl. 18, 1–158.

Guo, F., Fan, W.M., Wang, Y.J., Li, C.W., 2004. When did the Emeishan mantle plume activity start? Geochronological and geochemical evidence from ultrmafic–mafic dikes in southwestern China. Int. Geol. Rev. 46, 226–234.

Han, B.F., Wang, S.G., Jahn, B.M., Hong, D.W., Kagami, H., Sun, Y.L., 1997. Depleted-mantle source for the Ulungur River A-type granites from North Xinjiang, China: geochemistry and Nd–Sr isotopic evidence, and implications for Phanerozoic crustal growth. Chem. Geol. 138, 135–159.

Harris, N.B.W., Marzouki, F.M.H., Ali, S., 1986. The Jabel Sayid complex, Arabian shield: geochemical constraints on the origin of peralkaline and related granites. J. Geol. Soc. Lond. 143, 287–295.

He, B., Xu, Y.G., Chung, S.L., Xiao, L., Wang, Y., 2003. Sedimentary evidence for a rapid crustal doming prior to the eruption of the Emeishan flood basalts. Earth Planet. Sci. Lett. 213, 389–405.

Huang, K.N., Opdyke, N.D., 1998. Magnetostratigraphic investigations on an Emeishan basalt section in western Guizhou province, China. Earth Planet. Sci. Lett. 163, 1–14.

Huang, K.N., Opdyke, N.D., Kent, D.V., Xu, G.Z., Tang, R.L., 1986. Further paelomagnetic results from the Permian Emeishan basalts in SW China. Kexue Tongbao 31, 1192–1201 (in Chinese).

Jahn, B.M., Condie, K.C., 1995. Evolution of the Kaapvaal Craton as viewed from geochemical and Sm–Nd isotopic analyses of intracratonic pelites. Geochim. Cosmochim. Acta 59, 2239–2258.

Jahn, B.M., Wu, F.Y., Lo, C.H., Tsai, C.H., 1999. Crust–mantle interaction induced by deep subduction of the continental crust: geochemical and Sr–Nd isotopic evidence from post-collisional mafic–ultramafic intrusions of the northern Dabie complex, central China. Chem. Geol. 157, 119–146.

Jochum, K.P., Nohl, U., Herwig, K., Lammel, E., Stoll, B., Hofmann, A.W., 2005. GeoReM: a new geochemical database for reference materials and isotopic standards. Geostand. Geoanal. Res. 29, 333–338.

Kerr, A., 1994. Lithospheric thinning during the evolution of continental large igneous provinces: a case study from North Atlantic Tertiary province. Geology 22, 1027–1039.

Kerr, A., Fryer, B.J., 1993. Nd isotope evidence for crust–mantle interaction in the generation of A-type granitoids suites in Labrador, Canada. Chem. Geol. 104, 39–60.

Keto, L.S., Jacobsen, S.B., 1987. Nd and Sr isotopic variations of Early Paleozoic oceans. Earth Planet. Sci. Lett. 84, 27–41.

Le Maitre, R.W., Bateman, P., Dudek, Keller, A.J., Lameyre Le Bas, M.J., Sabine, P.A., Schmid, R., Sorensen, H., Streckeisen, A., Wolley, A.R., Zanetti, B., 1989. A Classification of Igneous Rocks and Glossary of Terms. Blackwell, Oxford. 193 pp.

Liu, D., Shen, F.K., Zhang, G.Z., 1985. Layered intrusions of the Panxi area, Sichuan province. In: Zhang, Y.X. (Ed.), Corpus of the Panxi Paleorift Studies in China. Geological Publishing House, Beijing, pp. 85–118 (in Chinese).

Liu, J.H., Liu, F.T., He, J.K., Chen, H., You, Q.Y., 2001. Study of seismic tomography in Panxi paleorift area of southwestern China—structural feartures of crust and mantle and their evolution. Sci. China, Ser. D Earth Sci. 44, 277–288.

Lo, C.H., Chung, S.L., Lee, T.Y., Wu, G.Y., 2002. Age of the Emeishan flood magmatism and relations to Permian–Triassic boundary events. Earth Planet. Sci. Lett. 198, 449–458.

Loiselle, M.C., Wones, D.R., 1979. Characteristics and origin of anorogenic granites. Geol. Soc. Amer. Bull. Abstr. Prog. 92, 468.

Mahood, G., Hildreth, W., 1983. Large partition coefficients for trace elements in high silica rhyolites. Geochim. Cosmochim. Acta 47, 11–30.

Martin, H., Bonin, B., Capdevila, R., Jahn, B.M., Lameyre, J., Wang, Y., 1994. The Kuiqi peralkaline granitic complex (SE China): petrology and geochemistry. J. Petrol. 35, 983–1005.

McDonough, W.F., Sun, S.-s., 1995. The composition of the Earth. Chem. Geol. 120, 223–253.

Milner, S.C., le Roex, A.P., 1996. Isotope characteristics of the Okenyenya igneous complex, northwestern Namibia: constraints on the composition of the early Tristan plume and the origin of the EM 1 mantle component. Earth Planet. Sci. Lett. 141, 277–291.

Nash, W.P., Crecraft, H.R., 1985. Partition coefficients for trace elements in silicic magmas. Geochim. Cosmochim. Acta 49, 2309–2322.

Patiño Douce, A.E.P., 1997. Generation of metaluminous A-type granites by low-pressure melting of calc-alkaline granitoids. Geology 25, 743–746.

Peccerillo, A., Barberio, M.R., Yirgu, G., Ayalew, D., Barbieri, M., Wu, T.W., 2003. Relationships between mafic and peralkaline silicic magmatism in continental rift settings: a petrological, geochemical and isotopic study of the Gedemsa Volcano, central Ethiopian rift. J. Petrol. 44, 2003–2032.

Potts, P.J., Kane, J.S., 2005. International association of geoanalysts certificate of analysis: certified reference material OU-6 (penrhyn slate). Geostand. Geoanal. Res. 29, 233–236.

Qi, L., Hu, J., Grégoire, D.C., 2000. Determination of trace elements in granites by inductively coupled plasma mass spectrometry. Talanta 51, 507–513.

Renne, P.R., Zhang, Z.C., Richards, M.A., Black, M.T., Basu, A.R., 1995. Synchrony and causal relation between Permian–Triassic boundary crises and Siberian Flood Volcanism. Science 269, 1413–1416.

Riley, T.R., Leat, P.T., Pankhurst, R.J., Harris, C., 2001. Origin of large volume rhyolitic volcanism in the Antarctic Peninsula and Patagonia by crustal melting. J. Petrol. 42, 1043–1065.

Rudnick, R.L., Fountain, D.M., 1995. Nature and composition of the continental crust: a lower crustal perspective. Rev. Geophys. 33, 267–309.

SBGMR (Sichuan Bureau of Geology and Mineral Resources), 1991. Regional Geology of Sichuan Province. Geological Publishing House, Beijing. 680 pp. (in Chinese).

Skjerlie, K.P., Johnston, A.D., 1992. Fluid-absent melting behaviour of an F-rich tonalitic gneiss at mid-crustal pressures: implications for the generation of anorogenic granites. J. Petrol. 34, 785–815.

Song, X.Y., Zhou, M.F., Hou, Z.Q., Cao, Z.M., Wang, Y.L., Li, Y.G., 2001. Geochemical constraints on the mantle source of the upper Permian Emeishan continental flood basalts, southwestern China. Int. Geol. Rev. 43, 213–225.

Song, B., Zhang, Y.H., Wan, Y.S., Jian, P., 2002. Mount Making and procedure of the SHRIMP dating. Geol. Rev. 48, 26–30 (Suppl., in Chinese).

Song, X.Y., Zhou, M.F., Cao, Z.M., Sun, M., Wang, Y.L., 2003. Ni–Cu–(PGE) magmatic sulfide deposits in the Yangliuping area, Permian Emeishan igneous province, SW China. Miner. Depos. 38, 831–843.

Sylvester, R.S., 1989. Post-collisional alkaline granites. J. Geol. 97, 261–280.

Tao, Y., Gao, Z.M., Luo, T.Y., Qi, J.D., He, Y.J., Yang, T.X., 2002. Inversion of primary magma composition for Jinbaoshan ultramafic intrusion, Yunnan. Acta Petrol. Sin. 18, 70–82 (in Chinese).

Taylor, S.R., McLennan, S.M., 1985. The Continental Crust: Its Composition and Evolution. Blackwell Scientific Publications, Oxford. 312 pp.

Taylor, R.P., Strong, D.F., Kean, B.F., 1980. The Topsails igneous complex: Silurian–Devonian peralkaline magmatism in western Newfoundland. Can. J. Earth Sci. 17, 425–439.

Tollo, R.P., Aleinkoff, J.N., Bartholomew, M.J., Rankin, D.W., 2004. Neoproterozoic A-type granitoids of the central and southern Appalachians: intraplate magmatism associated with episodic rifting of the Rodinian supercontinent. Precambrian Res. 128, 3–38.

Turner, J.S., Campbell, I.H., 1986. Convection and mixing in magma chambers. Earth Sci. Rev. 23, 255–352.

Turner, S.P., Foden, J.D., Morrison, R.S., 1992. Derivation of A-type magmas by fractionation of basaltic magma: an example from the Padthaway Ridge, South Australia. Lithos 28, 151–179.

Vernikovsky, V.A., Pease, V.L., Vernikovskaya, A.E., Romsnov, A.P., Gee, D.G., Travin, A.V., 2003. First report of early Triassic A-type granite and syenite intrusions from Taimyr: product of the northern Eurasian superplume? Lithos 66, 23–36.

Wager, L.R., Brown, G.M., 1968. Layered Igneous Rocks. Oliver and Boyd, Edinburgh. 588 pp.

Watson, E.B., Harrison, T.M., 1983. Zircon saturation revisited: temperature and composition effects in a variety of crustal magma types. Earth Planet. Sci. Lett. 64, 295–304.

Whalen, J.W., Currie, K.L., Chappell, B.W., 1987. A-type granites: geochemical characteristics, discrimination and petrogenesis. Contrib. Mineral. Petrol. 95, 407–419.

Wolff, J.A., Storey, M., 1984. Zoning in highly alkaline magma bodies. Geol. Mag. 121, 563–575.

Wu, F.Y., Sun, D.Y., Li, H.M., Jahn, B.M., Wilde, S.A., 2002. A-type granites in northeastern China: age and geochemical constraints on their petrogenesis. Chem. Geol. 187, 143–173.

Xiao, L., Xu, Y.G., Mei, H.J., Zheng, Y.F., He, B., Pirajno, F., 2004. Distinct mantle sources of low-Ti and high-Ti basalts from the western Emeishan large igneous province, SW China: implications for plume-lithosphere interaction. Earth Planet. Sci. Lett. 228, 525–546.

Xu, Y.G., Chung, S.L., Jahn, B.M., Wu, G.Y., 2001. Petrologic and geochemical constraints on the petrogenesis of Permian–Triassic Emeishan flood basalts in southwestern China. Lithos 58, 145–168.

Xu, Y.G., He, B., Chung, S.L., Menzies, M.A., Frey, F.A., 2004. Geologic, geochemical, and geophysical consequences of plume involvement in the Emeishan flood–basalt province. Geology 32, 917–920.

Yao, P.H., Wang, K.N., Du, C.L., Lin, Z.T., Song, X., 1993. Records of China's Iron Ore Deposits. Metallurgic Industry Press, Beijing, pp. 633–649 (in Chinese).

Yuan, X.C., 1996. Geophysical Maps of China. Geological Publishing House, Beijing. 200 pp. (in Chinese).

Zhang, Y.X., Luo, Y.N., Yang, C.X., 1988. Panxi Rift. Geological Publishing House, Beijing. 325 pp. (in Chinese).

Zhang, Z.Q., Lu, J.R., Tang, S.H., 1999. Sm–Nd ages of the Panxi layered basic–ultrabasic intrusions in Sichuan. Acta Geol. Sin. 73, 263–271 (in Chinese).

Zhong, H., Zhu, W.G., 2006. Geochronology of layered mafic intrusions from the Pan-Xi area in the Emeishan large igneous province, SW China. Miner. Depos. 41, 599–606.

Zhong, H., Zhou, X.H., Zhou, M.F., Sun, M., Liu, B.G., 2002. Platinum-group element geochemistry of the Hongge Fe–V–Ti deposit in the Pan-Xi area, southwestern China. Miner. Depos. 37, 226–239.

Zhong, H., Yao, Y., Hu, S.F., Zhou, X.H., Liu, B.G., Sun, M., Zhou, M.F., Viljoen, M.J., 2003. Trace-element and Sr–Nd isotopic geochemistry of the PGE-bearing Hongge layered intrusion, southwestern China. Int. Geol. Rev. 45, 371–382.

Zhong, H., Yao, Y., Prevec, S.A., Wilson, A.H., Viljoen, M.J., Viljoen, R.P., Liu, B.G., Luo, Y.N., 2004. Trace-element and Sr–Nd isotopic geochemistry of the PGE-bearing Xinjie layered intrusion in SW China. Chem. Geol. 203, 237–252.

Zhong, H., Zhu, W.G., Qi, L., Zhou, M.F., Song, X.Y., Zhang, Y., 2006. Platinum-group element (PGE) geochemistry of the Emeishan basalts in the Pan-Xi area, SW China. Chin. Sci. Bull. 51 (7), 845–854.

Zhou, B.F., Shi, Z.M., Zhang, Y.C., Li, X., 1985. A-type granites of the Panxi rift zone. In: Zhang, Y.X. (Ed.), Corpus of the Panxi Paleorift Studies in China. Geological Publishing House, Beijing, pp. 201–223 (in Chinese).

Zhou, M.F., Malpas, J., Song, X.Y., Robinson, P.T., Sun, M., Kennedy, A.K., Lesher, C.M., Keays, R.R., 2002. A temporal link between the Emeishan large igneous province (SW China) and the end-Guadalupian mass extinction. Earth Planet. Sci. Lett. 196, 113–122.

Zhou, M.F., Robinson, P.T., Lesher, C.M., Keays, R.R., Zhang, C.J., Malpas, J., 2005. Geochemistry, petrogenesis and metallogenesis of the Panzhihua gabbroic layered intrusion and associated Fe–Ti–V oxide deposits, Sichuan province, SW China. J. Petrol. 46, 2253–2280.